8 BP

EROSIONAL ASPECTS OF DIVERTER DESIGN

A Thesis

Submitted to the Graduate Faculty of the
Louisiana State University and
Agricultural and Mechanical College
in partial fulfillment of the
requirements for the degree of
Master of Science

in

The Department of Petroleum Engineering

by
Stephen A. Rohleder
B.S., University of Wisconsin, 1981
December 1985

ACKNOWLEDGEMENT

The author wishes to express thanks to Dr. Walter Whitehead, associate professor of petroleum engineering at Louisiana State University, for his guidance and constructive criticisms in the experimental work and the writing of this thesis. He would also like to thank Mr. Allen Kelly, Mr. James Sykora, Mr. John Vincent, and Mr. Joe Spradley of the LSU IADC Blowout Control School for their efforts in designing, troubleshooting, and repairing the flow loop equipment. Dr. William Holden, professor of petroleum engineering, is appreciated for assistance in calibrating the pressure and temperature sensors. Special thanks goes to Mr. Larry Hess and Mr. Jerome Paulson of the HammerTek Corporation for providing technical information about the Vortice-Ell. Dr. Mehdy Sabbaghian and Dr. Harvill Eaton, of the LSU Mechanical Engineering Department, are also appreciated for information they offered in the field of erosion. This study was supported in part by the United States Minerals Management Service, Department of the Interior. This thesis could not have been completed without the professional assistance and magic fingers of Karen Julian, typist extraordinaire.

TABLE OF CONTENTS

LIST OF TABLES

LIST OF FIGURES

ABSTRACT

Diverter systems are used on oil and gas drilling rigs to direct uncontrolled flow of formation fluids away from the rig. The system must function properly for long enough to evacuate the personnel from the rig. A common mode of failure is erosion of the pipe ells. In an effort to improve diverter designs, this study evaluated 6 different pipe ells for their resistances to erosion.

An experimental flow loop was constructed for testing the pipe ells in an erosive stream. The types of members tested were the 1) cast short radius ell, 2) cast long radius ell, 3) cast plugged tee, 4) cast Vortice-Ell, 5) welded short radius ell, and 6) welded plugged tee. A mixture of drilling mud and blasting sand was pumped through each pipe ell for 90 hours. The fittings were weighed and tested for wall thicknesses before and after running in the flow loop. The analysis, based on erosion pattern and weight changes, indicated that the short radius ell performed the best. The plugged tee ranked second, the long radius ell third, and the Vortice-Ell fourth.

CHAPTER ONE

INTRODUCTION

In the course of shallow drilling operations, there is always a time period when the well should not be closed on a threatening blowout. This occurs in the early stages of drilling the well when the casing has not been set to a depth were the formations are competent enough to keep an underground blowout from broaching to the surface. If the formation fluids were allowed to broach to the surface, the ground around the conductor pipe might give way and a large crater-like hole would develop. Foundation support for the entire rig would be lost and the rig would collapse and fall. Formation fluids at the surface pose a threat of catching on fire or creating a pollution problem.

When the diverter system is employed, the wellbore and formation fluids are allowed to flow to the surface and, just below the drilling floor, are directed away from the rig. A diverter system is composed of some means of changing the direction of flow from vertical to horizontal, usually with an annular packing element, and a pipe system that leads the flow away from the rig. Two "vent lines" insure that the fluids can be directed downwind of the rig. Figures 1 and 2 are sketches of typical diverter

systems. The diverter does not actually hold back the flow but, instead, directs it away from the rig.

The diverter is strictly a safety system. It must perform its duty for at least long enough to evacuate the rig personnel. Like all safety equipment, the diverter system should be well designed and properly maintained.

When diverter systems are assembled on drilling rigs, they are often one of the last systems to be installed and a cut-and-fit approach is generally employed. Some piping designs use short and long radius ells, plugged tees, and flexible hose to change the flow direction. From the statistics on diverter events, these poor designs have resulted in a high number of diverter failures whenever the systems are called on.

One of the most common modes of diverter failure is through erosion of its component parts. The material flowing through the diverter contains a high concentration of erosive material (formation sand) traveling at very high speeds. Erosion occurs predominately where the flow changes directions. If every part of the diverter system were maintained well and functioned properly, the erosive nature of the flow stream alone might limit the life of the vent line.

The purpose of this study was to evaluate different pipe ells (also known as pipe fittings) for their ability to withstand an erosive stream and recommend one fitting

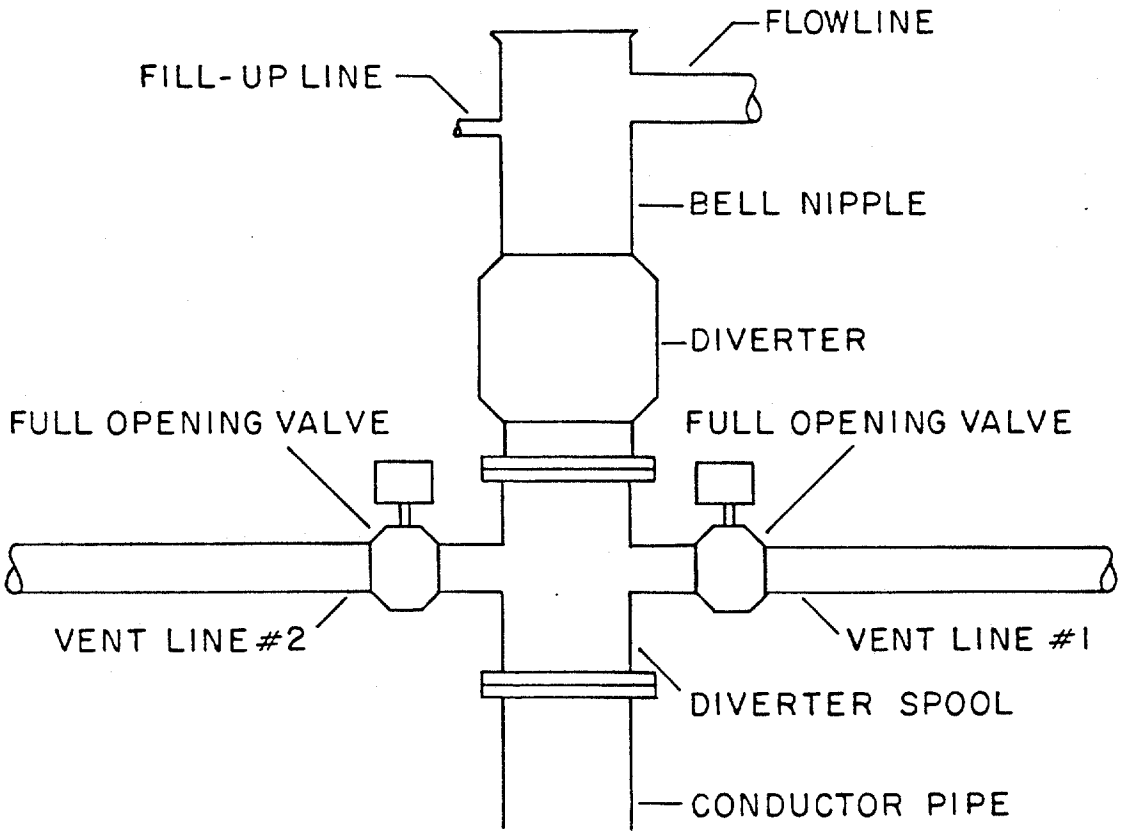

Figure 1. Example of a typical diverter system.

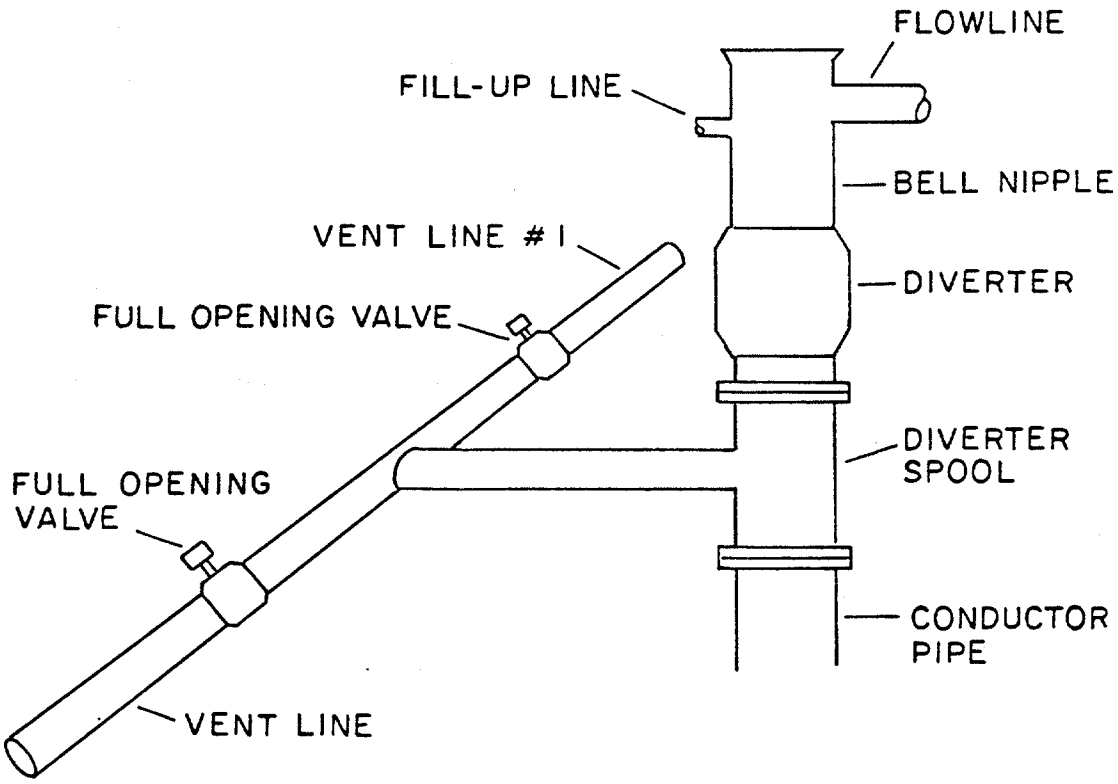

Figure 2. Example of a typical diverter system.

for use when the vent line must change directions. Six fitting designs were tested: the 1) cast short radius ell, 2) cast long radius ell, 3) cast plugged tee, 4) cast Vortice-Ell, 5) welded short radius ell, and 6) welded plugged tee. The 4 cast fittings are shown in figures 3, 4, 5, and 6. The first 3 fitting types are commonly found in the oil field whereas the Vortice-Ell is the trade name of a commercially available fitting made by the HammerTek Corporation. It is generally used in pneumatically conveyed materials-handling systems. The plugged tee is simply a pipe tee that is blanked off with a blind flange and positioned in the flow path so that the blind flange becomes a target, as shown in figure 7. The fittings were placed in an experimental flow loop that subjected them to an erosive stream of drilling mud and blasting sand. They were evaluated for their resistance to erosion based on 3 experimental criteria: 1) erosion pattern, 2) percent weight loss, and 3) weight loss divided by exposed surface area.

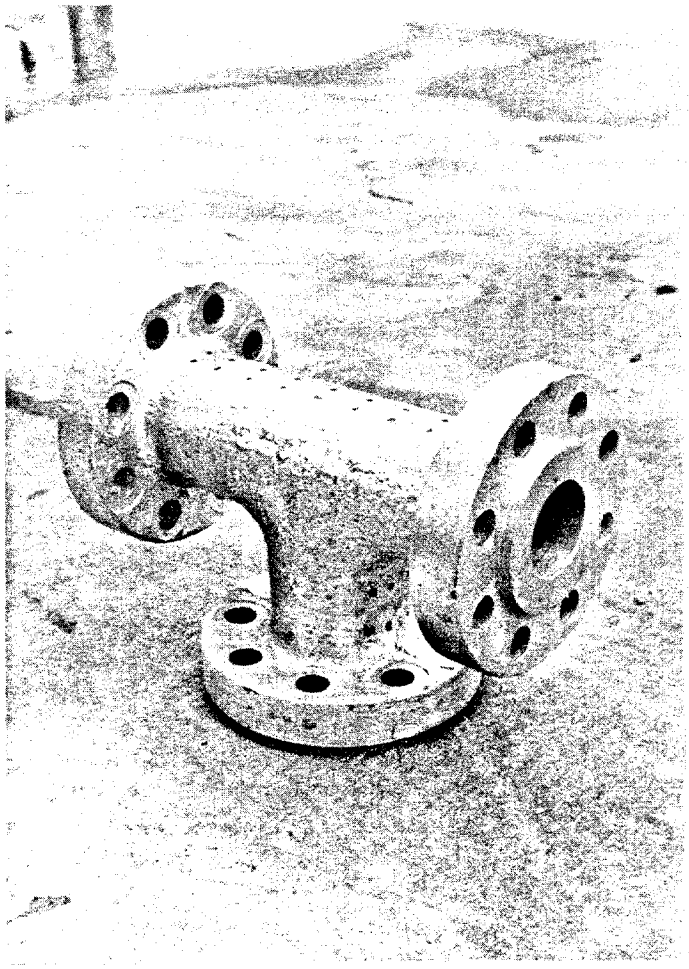

Figure 5. Plugged tee.

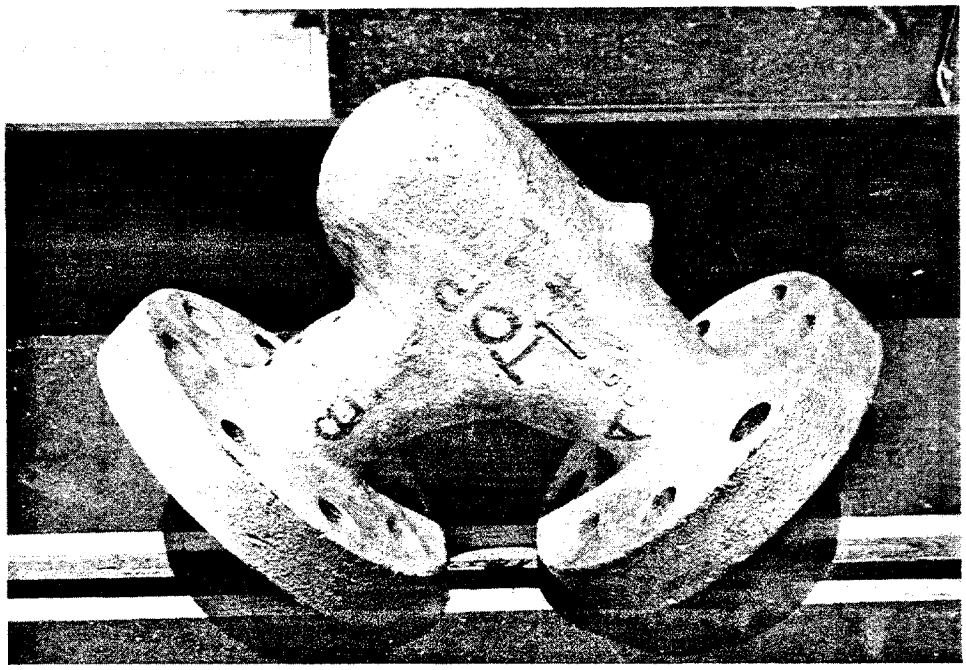

Figure 6. Vortice-Ell.

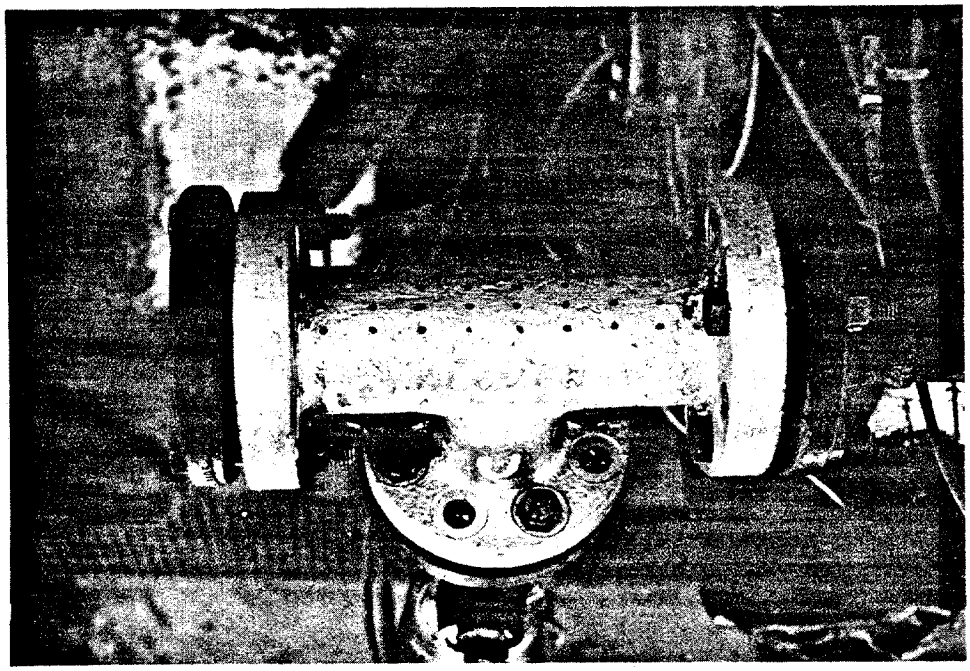

Figure 7. Plugged tee mounted in the flow loop.

CHAPTER TWO

LITERATURE REVIEW

2.1 Erosion: A Form of Abrasive Wear

2.1.1 Definitions and Types of Wear

Many investigators have studied the phenomenon of erosion and have tried to describe its behavior. Erosion is classified as a special form of wear. Eyre (1979) defines wear as the gradual loss of material from an object as it is subjected to constant friction forces. Wear is not a material property but is directly proportional to the amount of friction between the two contacting surfaces.

There are 5 different types of wear: 1) abrasive, 2) adhesive, 3) erosive, 4) fretting, and 5) chemical. This study discusses only abrasive and erosive wear. Abrasion involves the removal of material from one surface by the sliding action of a harder, acircular member (Eyre,1979). The result is a loss of material in parallel, grooved patterns from the softer member. Abrasive wear is important to this study because the grooves are the result of a cutting action. Erosion involves the same cutting action and is considered a special form of abrasive wear. Erosion is the removal of material from a surface that is being struck a multiple number of times by an impinging

material and abrasive microhardnesses are listed in Table 1.

Carbon content and microstructure

Serpik and Kantor (1965) showed how carbon content and microstructure affect a metals wear resistance, figure 10. Rate of cooling controls a steel's carbide size and, thus, its microstructure. Figure 11 shows how wear resistance decreases with increasing carbide size. Eyre (1975) found that the larger carbide crystals actually dislodge from the matrix. For a given carbon content, martensitic structured steels provide the greatest abrasion resistance because they have the least tendency to loose carbides.

2.1.3 Material Treatments

The wear resistance of an object can be improved either by choosing a highly resistive base material or by treating an inferior base metal. Surface treating is often cheaper than making the object entirely out of specialty materials. There are 3 main groups of surface treatments: surface deposition, surface hardening, and conversion coatings. Surface deposition is the process of applying additional amounts of material to the object (Eyre,1979). Some examples include hard facing, electrodeposition, and plasma spraying. Hard facing puts relatively thick layers of protective material on the base metal. The thick layers make this the most beneficial form of surface treatment in

TABLE 1

MATERIAL HARDNESS VALUES

	Microhardness Number	
mineral	Knoop	Vickers
feldspar	550	600-750
orthoclase	620	
quartz	840	900-1280
silicon carbide	2585	2600
diamond	7575	10000
material		
ferrite	235	70-200
pearlite, unalloyed		250-320
austenite, 12% Mn	305	170-230
martensite	500-800	500-1010
chromium carbide $(Fe,Cr)_7C_3$	1735	1200-1600
tungsten carbide WC	1800	2400
vanadium carbide VC	2660	2800
titanium carbide TiC	2470	3200
boron carbide B_4C	2800	3700

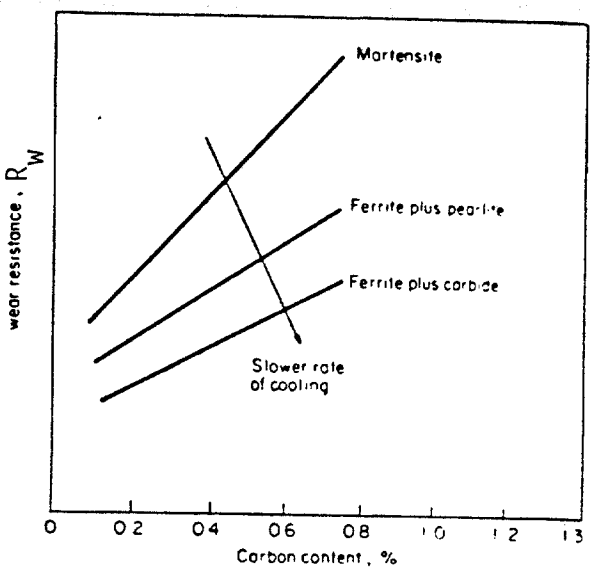

Figure 10. Effect of carbon content and microstructure on abrasive wear resistance of steels. (After Serpik and Kantor,1965)

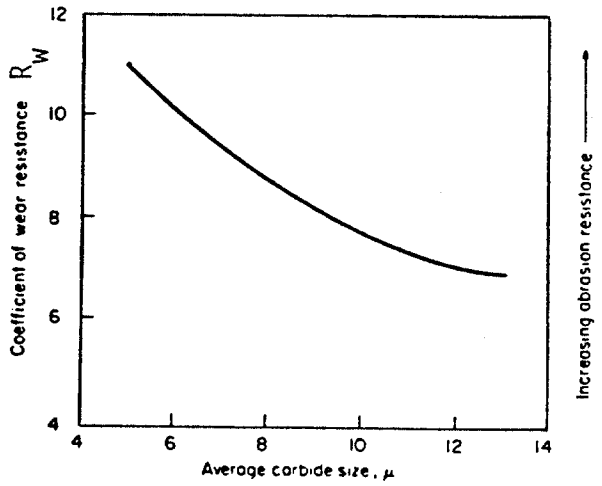

Figure 11. Effect of carbide particle size on abrasive wear resistance of white cast irons. (After Eyre,1975)

terms of increasing abrasion resistance. Surface hardening and conversion coating alter such thin layers that abrasion resistance is not improved for long periods of time.

The increased abrasion resistance of a surface treated member remains even after the altered layer has been removed. The altered layer creates a better run-in surface by making changes in the surface topography, hardness, and microstructure.

Despite the benefits gained from surface treatments, many designers feel that thicker base material ("beefing up" a member) assures greater resistance to wear or erosion failure.

2.2 Elements of Erosion

2.2.1 Definitions of Erosion

As mentioned earlier, erosion is a special form of abrasive wear. Both involve the loss of material by a cutting or gouging action. Erosion, W, is usually expressed as

$$W = \frac{\text{weight loss of target}}{\text{weight of material impacting target}}$$

Another commonly used expression is volumetric erosion, W_v, defined as

$$W_v = \frac{\text{erosion volume}}{\text{density of the target material}}$$

Volumetric erosion is used for comparing erosion between

two target materals that have different densities.

2.2.2 Types of Erosion Tests

Many types of tests have been developed for studying the factors that affect erosion and for defining the mechanisms that cause erosion: simulative tests, single impact tests, and laboratory tests.

Simulative tests

Simulative tests use full-scale models of a target object and subject it to a controlled erosive environment. The input environment is changed and the target's responses are recorded and analysed. This type of experimentation is possible only on systems where the input stimuli can be controlled very closely and where changes in one input do not alter another. Experimentation with pneumatic conveying systems indicated that erosion of pipe ells should be evaluated with erosion pattern as well as magnitude of material loss (Mason and Mills,1977). If erosion occured in a small, concentrated area and continued until a hole developed in the pipe, the ell would fail and only a small amount of material would be lost. This thesis used a full-scale model for testing the erosion resistance of several pipe ells and evaluated the ells on the basis of erosion pattern and weight loss.

Laboratory tests

Laboratory tests are used, primarily, to define the relationships between erosion and input parameters. The input parameters must be maintained at known and constant values. Ideally, a change in one input does not change another input. By studying several input/erosion response relationships, the mechanisms of erosion can be discerned and mathematical models developed. These type of experiments most commonly use "blast chamber" set ups where the erosive particles are fed into a tube, allowed to accelerate through a nozzle, and strike the target specimen. Particle velocity is generally measured with the use of high speed photography.

Single impact tests

Single impact tests study the effects of collisions between a single particle and the target. The goal of these experiments is to accurately describe the mechanisms of material removal. The impacting particle is fired at the target from a gas gun and is often of relatively large size.

2.2.3 Factors That Affect Erosion

These erosion tests have helped investigators define the factors that affect erosion. Some input variables include: 1) particle velocity, 2) particle hardness, 3) angle of impact, 4) duration of exposure, 5) aerodynamic

effects, 6) abrasives concentration, 7) temperature, and 8) tensile stress of the target member.

Minor influencing factors

Tilly (1969) found that particle concentration, target temperature, and tensile stress only slightly affected the magnitude of erosion. As particle concentration increased, the number of collisions (between particles) increased, and the amount of specific erosion decreased. The shape of the eroded channel narrowed and the target eroded in a smaller area.

Particle aerodynamics

Some input variables exhibit strong interrelationships with the other variables. Figure 12 shows how the flow path of a particle is altered as it approaches an inclined plate. Larger sized particles deviate less from the straight flow path and only particles twenty microns or larger actually strike the target at the intended angle. Using mathematical models, Tilly (1969) calculated the theoretical particle velocity and impact angle of particles striking an inclined plate, figure 13. These figures illustrate how a change in one parameter (plate angle) can affect other variables (velocity or actual impact angle). Strike efficiency is defined as the number of particles that strike a target divided by the number of particles initially aimed at the target. The effects of particle

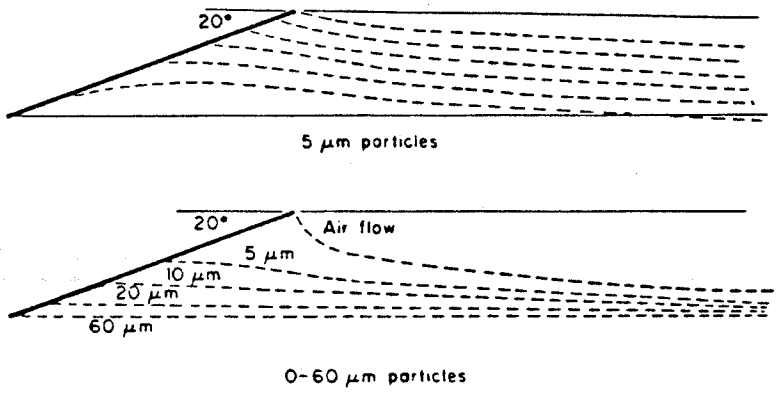

Figure 12. Particle flow approaching an inclined plate at 100 m/sec. (After Tilly,1969)

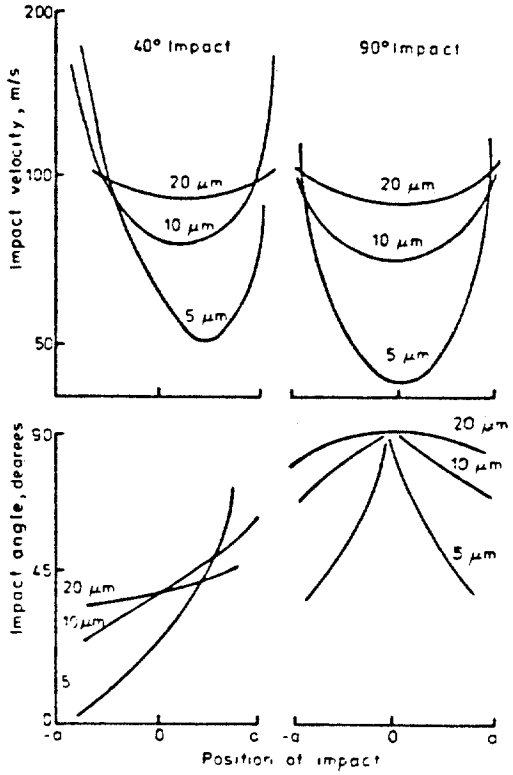

Figure 13. Influence of airflow on impact velocities and angles against inclined plates at 100 m/sec nominal velocity. (After Tilly,1969)

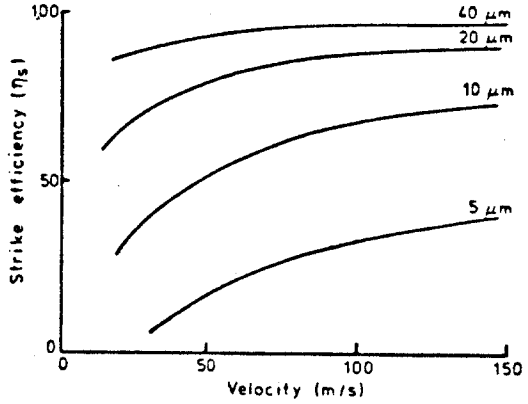

Figure 14. Influence of particle velocity and diameter on strike efficiency against a cylinder. (After Tilly,1969)

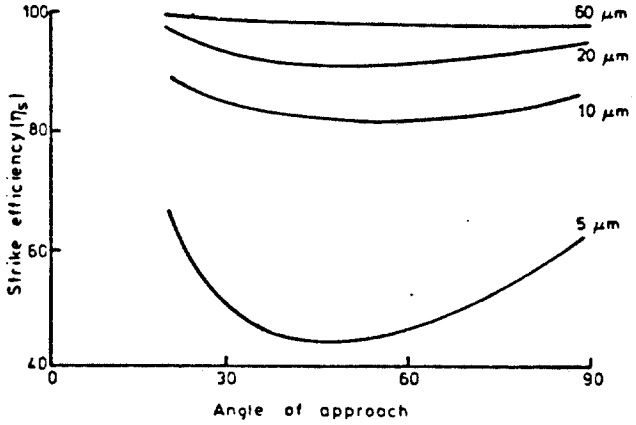

Figure 15. Variation on strike efficiency with angle of approach and particle velocity for flat plates at 100 m/sec nominal velocity. (After Tilly,1969)

velocity and angle of approach on strike efficiency are shown in figures 14 and 15, respectively. From this discussion, it is easy to see that the factors that influence erosion are often interrelated with one another.

Particle hardness

Sage and Tilly (1969) found that the hardness of the particle itself influenced the erosiveness of the abrasive stream. Erosion and Vicker's microhardness number, H_v, varied as

$$W = C * H_v^{2.3}$$

where C is a constant of proportionality.

Particle size

Erosion is also dependent on the impacting particle's size. There is a saturation level of erosion, W_{sat}, where the amount of erosion stays constant with increasing particle size (Sheldon and Finnie,1966). Also, for a given particle velocity, there is a threshold particle diameter below which smaller sized particles will not cause erosion. Erosion of ductile materials is related to the threshold particle diameter by the equation

$$W = W_{sat} * \left(1 - \left(\frac{d_o}{d}\right)^{1.5}\right)^2$$

where W = erosion,

W_{sat} = saturation level of erosion,

d = particle diameter,

d_o = threshold particle diameter.

Particle velocity

Many investigations have shown the relationship between particle velocity and erosion as

$$W = C * V^n$$

where C = constant,

V = particle velocity,

n = velocity exponent.

The study by Finnie (1960) found n = 2.0 when the target was SAE 1020 steel. Later work with ductile materials found n to vary between 2.3 and 2.4 (Tilly,1969) and (Behrendt,1970). Low velocity tests are used to determine threshold velocities below which material deformation is entirely elastic and no erosion occurs.

Impingement angle

The study by Bitter (1963a and b) showed that ductile materials undergo large erosional losses under glancing angles of impact. Maximum erosion in steels occured at impingement angles between twenty and thirty degrees. Brittle materials underwent maximum erosion at normal angles of attack. Figure 16 is a graph of erosion versus impact angle. The curve labeled "aluminum" shows the

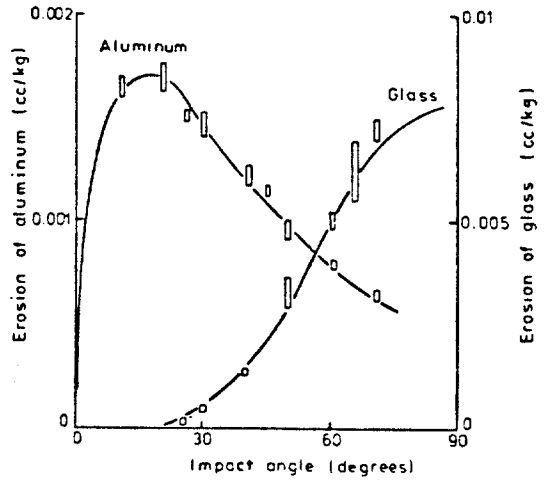

Figure 16. Effect on impact angle for 300 micron iron spheres at 10 m/sec. (After Bitter,1963)

typical response of ductile materials. Erosion increases rapidly from zero angle of attack through thirty degrees. The angle where maximum erosion occurs is designated α_o. As impact angle is increased past thirty degrees, erosion decreases. This response typifies a ductile material's erosion resistance to particle impacts at normal angles. A perfectly ductile material theoretically undergoes no erosion at 90 degrees. The curve labeled "glass" illustrates the typical response of a brittle material. Materials with very large microhardness numbers are often brittle. Little or no erosion occurs at glancing angles of attack and erosion increases to a maximum value at or near 90 degrees. These curves are described by the equation

$$W = A * \cos^2(\alpha) * \sin(n\alpha) + B * \sin^2(\alpha)$$

where A = ductility constant of the target material,

B = brittleness constant of the target material,

α = angle of impact,

$n = \frac{\pi}{2\alpha}$

α_o = angle of impact for maximum erosion.

If a materal is fully brittle, A = 0. If a material is fully ductile, B = 0. Most materials exhibit some degree of ductility and brittleness, so, at glancing angles, the ductile term will dominate and, at normal angles, the brittle term will dominate. Figure 17 is an example of erosion versus impingement angle for a material that shows

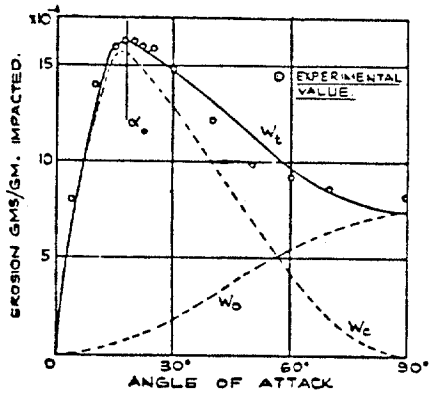

Figure 17. Influence of angle of attack on erosion. (After Neilson and Gilchrist,1968a)

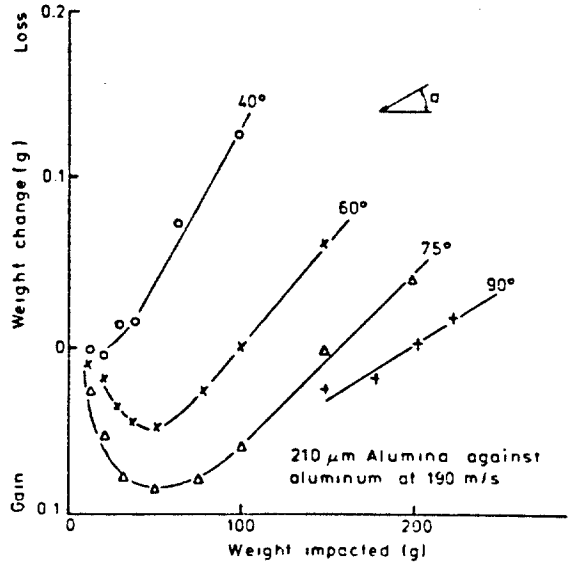

Figure 18. Variation of weight change with duration of erosion for different impact angles. (After Neilson and Gilchrist,1968a)

brittle and ductile behavior. In this graph, the total erosion curve has been separated into its ductile and brittle components.

2.2.4 Material Incubation Period

Early in an erosional process, the target material usually goes through some type of incubation period. Neilson and Gilchrist found that, during this time, the rate of erosion increases rapidly before stabilizing to a steady-state rate (1968a). After the incubation period, the erosion rate varied linearly with time. When ductile materials were subjected to normal angles of attack, there was an initial period when the abrasive embeded into the target material. Erosion and deposition occured at the same time. When the surface became saturated with abrasive fragments, erosion began to exceed deposition and weight loss occured. Figure 18 is a plot of target weight change versus mass of impacting particles for a ductile material. The curves indicate that the target gained weight early in the test. The greatest weight gains occured at higher impact angles. Glass and steel show steady-state erosional rates almost immediately, whereas softer materials, like aluminum, have considerable incubation periods. All analyses of erosion rate must be done during the steady-state period.

CHAPTER THREE

PREVIOUS INVESTIGATIONS

3.1 Mechanisms and Models of Erosion

3.1.1 Work Hardening and Chipping Mechanism

From the studies presented in the previous chapter, several investigators have suggested basic mechanisms that describe erosion. The earliest theory on erosion mechanics was that, after the particles struck the target, the material work hardened, became brittle, and chipped away under further impacts (Neilson and Gilchrist,1968a). The particles had to have enough energy to exceed the elastic limit of the work hardened materal.

3.1.2 Brittle and Ductile Mechanism

In an early work, Bitter (1963a and b) proposed that material loss resulted from 2 types of erosion: brittle and ductile. The brittle erosion process proceeds in the following manner: the impacting particle creates "Hertzian" stresses in the hard target material, the stresses produce cracks that extend radially from the impact area, the cracks combine, and the material dislodges by a subsequent impact. This type of erosion is described by the equation

$$W_b = a * (V * \sin(\alpha) - K)^n$$

where W_b = brittle erosion,

a = material constant,

V = particle velocity,

K = threshold velocity,

n = velocity exponent.

Velocity exponent ranges from 2.Ø to 2.2. The threshold velocity of most materials is negligibly small.

Ductile erosion was described as a cutting phenomenon where the particle scarred the target surface and extruded the material to the sides. The ridges of extruded material were then subject to further impacts. The 2 types of erosion were combined to give the expression

$$W = W_b + W_d$$

where W_d = ductile erosion.

If $W_{9Ø}$ is the erosion measured at 9Ø degrees and K is set to zero, this equation takes the form

$$W = W_{90} * \sin^n(\alpha) + W_d$$

By measuring the total erosion at other angles, the amount of ductile erosion can be calculated from

$$W_d = W - W_b$$

This model agreed well with experimental results. Under 9Ø degree impacts, brittle erosion increased with increasing hardness and ductile erosion decreased with increasing

hardness.

3.1.3 Cutting Mechanism

Finnie (1960) described ductile erosion as a cutting action where the sharp particles removed chips of the target material. For glancing impacts he developed the equation

$$W_1 = \frac{mV^2}{P\psi K} * \left[\sin(2\alpha) - \frac{6}{C} * \sin^2(\alpha)\right]$$

for $\alpha > \alpha_o$

where m = mass of the particle,

P = plastic flow stress,

ψ = ratio of depth of contact to depth of cut,

C = a constant.

The cutting action stops when the particle begins to leave the surface. For impact angles greater than , Finnie developed the equation

$$W_2 = \frac{mV^2}{6P\psi} * \cos^2(\alpha)$$

In this equation, cutting stops when the particles' kinetic energy equals zero. In both of these equations the particle is assumed to remain intact. This model correlates well with ductile erosion at glancing angles and predicts zero erosion at 90 degree angles but is generally not used due to the complexity of its terms.

3.1.4 Cutting and Deformation Mechanism I

Bitter (1963a) developed a cutting model for ductile erosion based on energy balance. He found

$$W_{c1} = \frac{2MC * (V * \sin(\alpha) - K)^2}{(V * \sin(\alpha))^{\frac{1}{2}}} * \left(V * \sin(\alpha) - \frac{C * q * (V * \sin(\alpha) - K)^2}{(V * \sin(\alpha))^{\frac{1}{2}}}\right) \quad \text{for } \alpha \leq \alpha_o$$

and

$$W_{c2} = \frac{M}{2q} * \left(V^2 * \cos^2(\alpha) - K_1 * (V * \sin(\alpha) - K)^{1.5}\right) \quad \text{for } \alpha \geq \alpha_o$$

where W_{c1} = cutting erosion for $\alpha < \alpha_o$,
W_{c2} = cutting erosion for $\alpha > \alpha_o$,
M = total mass of the impacting particles,
C and K_1 = constants,
K = velocity component normal to the target below which no erosion takes place,
q = cutting wear factor.

Maximum erosion occurs at α_o where $W_{c1} = W_{c2}$. Bitter combined cutting erosion with another expression for brittle erosion which he termed deformation erosion. Deformation erosion has the form

$$W_D = \frac{M * (V * \sin(\alpha) - K)^2}{2 * \varepsilon}$$

where W_D = deformation erosion,
ε = deformation wear factor.

The combination of equations

$$W = W_c + W_D$$

predicts the amount of erosion that would occur at any angle. Unfortunately, some of the terms in both equations are very complex. The complexities of this model have spurred other researchers to develop more practical equations.

3.1.5 Cutting and Deformation Mechanism II

Neilson and Gilchrist (1968) developed an emperical model based on energy balance and the conclusions drawn from the Bitter and Finnie experiments. Their equations that describe the curves of figure 17 are

$$W = \frac{M * V^2 * \cos^2(\alpha)}{2 * \Phi} + \frac{M * (V * \sin(\alpha) - K)^2}{2 * \varepsilon}$$

for $\alpha \geq \alpha_o$

and

$$W = \frac{M * (V^2 * \cos^2(\alpha) - V_p^2)}{2 * \Phi} + \frac{M * (V * \sin(\alpha) - K)^2}{2 * \varepsilon}$$

for $\alpha \leq \alpha_o$

where Φ and ε = units of kinetic energy that must be absorbed by the target to release one unit of eroded material,

Φ = cutting wear factor,

ε = deformation wear factor,

V_p = residual parallel component of particle velocity at small angles of attack,

α_o = impact angle where $V_p = \emptyset$.

In this equation, K is so small that it is taken to be zero. The values of Φ and ε are obtained experimentally. For entirely brittle materials, the cutting wear factor goes to infinity and for entirely ductile materials, the deformation wear factor goes to infinity. The cutting and deformation wear factors can be used to predict a material's erosion response. If Φ/ε is greater than one, the deformation wear term dominates and the material should exhibit primerily brittle material responses. If Φ/ε is less than one, the cutting wear term dominates and the target should show a more ductile response. These equations predict erosion responses that agree well with experimental data.

3.1.6 Two Stage Mechanism

Tilly's (1973) used a 2 stage mechanism to describe erosion. The first stage is when the particles strike the target surface, create indentations along their travel paths, and extrude material to the sides forming lips along the indentation. The lips are removed as chips upon further impacts. The second stage of erosion is when the particle breaks up into fragments, the fragments project radially from the primary site, and scour the target

surface. Large particles and high velocities cause the greatest fragmentation, thus, increases in particle size and velocity increases secondary erosion. Particles that are too small to break up any further cause primary erosion only.

The primary erosion model was developed from Bitter's conservation of energy equation. The energy available to erode a specimen is expressed in terms of threshold velocity and threshold particle size. From this analysis Tilly developed the equation

$$W_1 = W_1' * \left(\frac{V}{V_r}\right)^2 * \left(1 - \left(\frac{d_o}{d}\right)^{1.5} * \frac{V_o}{V}\right)^2$$

where W_1 = primary erosion at any velocity greater than threshold,

W_1' = primary erosion observed during the test,

V_r = test velocity,

V_o = threshold particle velocity.

V = any other velocity where $V >> V_o$ and $d >> d_o$.

Secondary erosion is a function of the degree of fragmentation and is expressed by the equation

$$W_2 = W_2' * \left(\frac{V}{V_r}\right)^2 * F_{d,r}$$

where

$$F_{d,r} = \frac{Wt_o - Wt}{Wt_o}$$

where W_2 = secondary erosion at any velocity greater than threshold,

W_2' = secondary erosion observed during test,

$F_{d,r}$ = degree of fragmentation,

Wt_o = proportion of sample (by weight) within a specified size range before testing,

Wt = proportion of sample (by weight) within a specified size range after testing.

Primary and secondary erosions are combined in the equation

$$W = W_1 + W_2$$

Primary erosion dominates at glancing angles of attack and secondary erosion dominates at normal angles. The model correlate well with experimental data for 90 degree impacts and a wide range of particle sizes. The equations use a power law relation between velocity and erosion where n > 2.0, which is consistant with the literature. At higher velocities and larger particle sizes, threshold conditions have less influence, fragmentation becomes a maximum, and n approaches 2.0.

3.2 Applications of the Models

3.2.1 Purpose of the Laboratory Experiments

All of the above described experiments were performed with the end purpose of describing the mechanisms of erosion and predicting erosion behavior with mathematical

models. All of these models were developed from blast tube or whirling arm type experimental rigs. These apparati afforded good control over the input variables (angle of impact, particle velocity, particle size, etc.). Their results proved reproducible and the models described the data well.

3.2.2 Purpose of This Study

The aim of this project was to evaluate several different pipe bends for their relative erosion resistances. This project examined a whole system from an erosional standpoint and did not look into the mechanisms of erosion. Experiments done by the other investigators could not be used to test the pipe bends. Their experiments tested small pieces of metal for targets, not pipe ells with flanges attached. It was obvious that a new test setup was needed.

3.2.3 Inability to Apply the Models

The erosion models also proved inapplicable to this study. Some of the input variables, such as impact angle, particle velocity, and strike efficiency, could only be obtained with blast tube and whirling arm type equipment. Angle of attack was undefined in this work because the erosive stream underwent a sweeping 90 degree change in direction. The laboratory experiments used high speed photography to measure particle velocity. With a slurry

flow, the particle velocity could only be calculated. All of the models were developed with the abrasive traveling through air or a vacuum, but this study used liquid as the carrying fluid. This experiment used a particle size that varied over a much wider range than the laboratory experiments. The mathematical models often require experimental values obtained from calibration test runs. These calibration values can only be obtained from laboratory type experiments.

3.2.4 Alternate Experimentation and Evaluation

For these reasons, the pipe ells were tested with an entirely different experimental setup. The ells were mounted in a flow loop and an abrasive fluid was pumped through the system. Erosion was evaluated by 3 means: 1) erosion pattern, 2) weight loss divided by exposed surface area, and 3) percent weight loss. Since abrasive concentration controls the width of the eroded channel, erosion pattern became the primary evaluation criterion. Percent weight loss was used because the standard definition of erosion could not be applied. And weight lost per exposed surface area accounted for material loss at the flanges. Further justification of these criteria are presented in the results chapter.

CHAPTER FOUR

EXPERIMENTAL APPARATUS

4.1 Equipment

4.1.1 Experimental Setup

An experimental flow loop was constructed to simulate formation fluids blowing out through a diverter system. Figure 19 is a sketch of the experimental setup. Drilling mud flowed from the right side of the tank to the pump, through 20 feet of 2 inch inside diameter pipe, through the pipe ell, and back into the tank. The pipe ell was the erosional target of this whole experiment. Blasting sand was added to the mud to simulate formation sand being carried through the diverter. A Harrisburg 178, 5x6 inch centrifugal pump was used to move the slurry through the flow loop.

4.1.2 Abrasive Slurry

The mud was a simple mixture of bentonite clay, caustic soda, and water. The clay raised the viscosity of the mud and held the sand in a suspension. Number 2 blasting sand was chosen as the abrasive because it is well graded and more closely simulates formation sand than #1 blasting sand. Two propeller type mud agitators were installed in the tank in order to keep the sand from

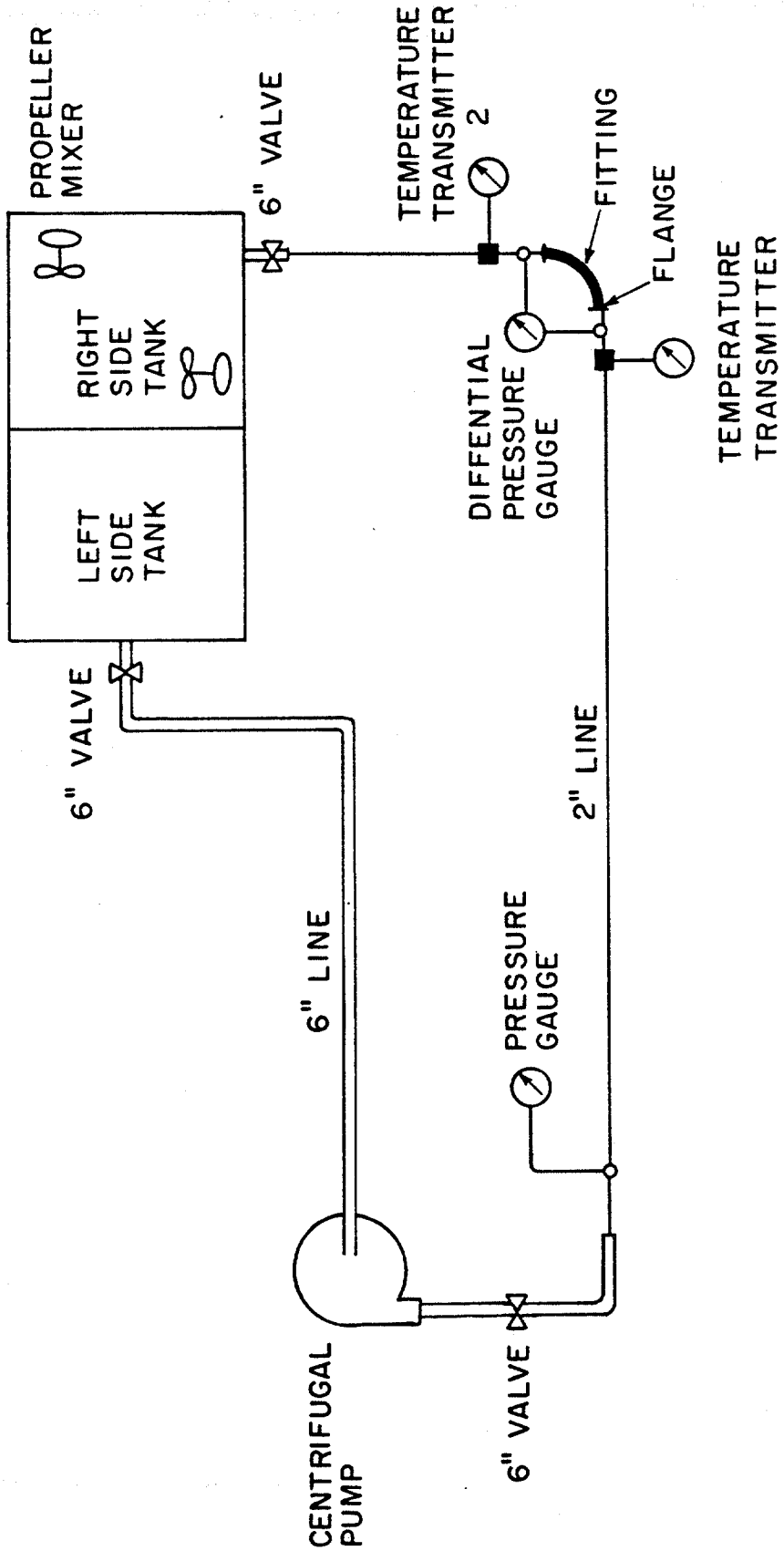

Figure 19. Schematic of the flow loop experimental setup.

settling. In a further effort to keep the sand suspended, only the right side of the tank was filled with mud. By sucking and discharging from just the right side of the tank and leaving the left side empty, the mud was subjected to much more turbulence. All attempts were made to insure that the slurry had a smooth flow pattern as it reached the fitting. The 20 feet of flowline helped reduce the pump effects. All weldment burrs in the flowline were ground smooth. And raised face flanges provided smooth connections between the flowline and the fittings.

4.1.3 Fitting Types

Six different types of fittings were tested; 1) cast short radius ell, 2) cast long radius ell, 3) cast plugged tee, 4) cast Vortice-Ell, 5) welded short radius ell, and 6) welded plugged tee. The first 4 fittings had their flanges cast integrally with the pipe member in order to provide a very smooth connection surface. The welded fittings had their flanges welded onto the pipe member.

4.2 Measurements

4.2.1 Measurements of Erosion

The pipe fitting was weighed once before and once after running through the flow loop. The scale, an Accu-Weigh III, model 301 TDX, had a rated sensativity of 0.01 pounds. The wall thickness of the pipe fittings were measured using an ultrasonic thickness device. Comparison

of wall thicknesses before and after the test gave insights into the wear pattern of each fitting.

4.2.2 Flow Loop Data

Several measurements were taken while the experiment was being run. These include flow rate, flowline pressure, differential pressure across the fitting, temperatures upstream and downstream of the fitting, sand content, and mud properties. The procedure for recording these data is discussed in the following paragraphs.

Flow rate

Flow rate was measured by recording the change in height of the mud level in the tank after a certain amount of pumping time. Under normal running operations, the left tank was left empty and the right tank was always full of mud. Certain valves were opened that allowed the mud to flow from the right tank to the left tank until their levels equilibrated. The suction line from the right tank was then closed causing the pump to draw from the left side only. Since the flow loop discharged into the right tank only, the mud level in the left tank dropped and that in the right tank rose. By measuring the change in fluid level, the time elasped, and the tank dimensions, the pump flow rate was easily calculated. The whole process was repeated 3 times and an average value taken.

water tended to "boil" out of the slurry. A small sample was collected in a special sand content tube which gave sand content from graduations on the bottom of the tube. After monitoring the mud, corrective measures could be taken to return the slurry properties to their desired values. These small samples were not used to find the slurry's true sand content because, it was felt, the larger samples were more representative.

Pressures and temperature

Flowline pressure was measured using a Gould, series PG 3000 pressure transducer. The transducer was located just downstream of the pump on the 2 inch flowline. Differential pressure across the pipe fitting was measured with a Rosemount, type 1151 DP differential pressure cell. Fluid ports were drilled in the flow loop 4 inches upstream and downstream of the fitting flanges. Two RdF Corporation, series 2600 temperature transmitters were placed 1 foot upstream and downstream of the fitting flanges. The temperature sensors were strapped to the outside of the flowpipe and wrapped with insulation material.

All of the electronic sensors were calibrated in the lab to a zero response of 4 milliamps and a high range response of 20 milliamps. An operating voltage of twenty volts DC was applied to the instruments, their measuring

signal channeled through a 4 channel switch, and the return current signal measured with a Fluke ammeter. The ammeter readings were entered into a handheld calculator that was programmed to convert the milliamp responses into pressure and temperature values. The program used the linear responses of the instruments as defined by the zero and range readings.

4.2.3 Choice of Materials Used

The types of steel, sand, and mud chosen for this experiment were selected on the basis of their availability to both the industry and the experiment. All fittings were made of steel with ASTM specification A216, grade WCB. This is a common grade of steel and is frequently used for oil field tubulars. Using a soft steel allows the experiment to examine a worst-case diverter system. The soft steel also eroded faster, making the results more dramatic. The sand was commercially available #2 blasting sand and had a large range of grain sizes. The simple drilling mud provided the fluid viscosity necessary for keeping the sand in suspension.

CHAPTER FIVE

EXPERIMENTAL PROCEDURE

5.1 General Procedure

The entire experimental method proceeded as follows. The outside of the fittings were painted with a rust proofer and the thickness measurement locations painted on. The fitting was then weighed, ultrasonically tested, and flanged up to the flow loop. A premixed volume of mud was pumped from a mud storage tank to the flow loop tank and a known volume of #2 blasting sand was added to the mud. The centrifrigal pump was turned on and pressure, differential pressure, temperatures, flow rate, sand content, and mud properties were mesured. Every 24 hours these measurements were taken again and any mud conditioning was done. Each fitting was run for a total of 90 hours circulation time. The fitting was then removed from the flow loop, washed, re-weighed, and re-thickness tested. With each new fitting, the mud and sand were replaced to insure that each fitting was subjected to the same erosive stream.

5.2 Changes Made on the Original Setup

Several changes were made to the original equipment setup. Each change was made in response to a particular

problem that arose. Fortunately, most of the changes were made while testing the welded short radius ell, test Run #1. This was considered a trial run expressly for ironing out any experimental problems.

Run #1 was a test of a short radius fitting with the flanges welded on. The original set up included 1 centrifugal pump with a 9 inch impeller. The flow rate over a run time of 62 hours run time was 7.24 gallons per minute. The fitting weight loss was low and the ultrasonic thickness test showed a maximum of 0.03 inches of pipe wall material removed. The results of Run #1 were discouraging, to say the least. This small amount of erosion demanded that changes be made to the original setup.

Two pumps in parallel

The first change was to add a second centrifugal pump in parallel with the first pump. This pump also had a 9 inch impeller. Table 2 lists the pressures and flow rates delivered by the pumps.

TABLE 2

NINE INCH IMPELLER OUTPUTS

	flowline pressure (psi)	flowrate (bbl/min)
pump #1	27.8	7.22
pump #2	28.7	7.58
combo	28.7	7.67

The above data indicates that the flow rate was not raised significantly by adding a second pump in parallel with the first.

Twelve inch pump impellers

The next change was to swap-out the 9 inch impellers for two 12 inch impellers. Table 3 lists the pressures and flow rates of each pump run alone and in combination.

TABLE 3

TWELVE INCH IMPELLER OUTPUTS

	flowline pressure (psi)	flowrate (bbl/min)
pump #1	48.Ø	1Ø.96
pump #2	46.5	1Ø.48
combo	47.2	11.2Ø

A significant increase in flow rate was realized by changing from a 9 inch to a 12 inch impeller. Since flow rate remained essentially unchanged when the pumps were run separately or in combination, it was logical to run only one pump at a time.

The benefits gained from using the 12 inch impeller were immediately realized. The welded short radius ell was mounted back in the flow loop. After only 67 hours, the ell eroded and a hole developed. The plots for this run,

presented at the end of the Appendix, dramatize the effects of changing from a 9 to a 12 inch impeller.

Preset Testing Time

The 2 pumps were run alternately for 24 hour periods. When not in use, the idle pump was isolated from the flow loop by closing a butterfly valve at the discharge line. Run #2, the welded plugged tee, was terminated early when one of the pump housings developed a hole and all the mud/sand slurry was pumped out of the system. The exact time that this happened was not known, but did develope some time after the system was checked that night. So the elapsed time for this run was known to only plus or minus 4 hours. Fortunately, the welded plugged tee was just considered another trial run. After this problem, the flow loop was converted back to a 1 pump system with one 12 inch impeller.

During Run #1, the pumps were only run during the day. Pressure and temperature measurements and mud samples were taken all throughout the day. Since these parameters changed very little in a day's time, the move to one suite of measurements per day was justified. Also, by running the pump continuously, some variations in the data were eliminated. The mud did not cool off overnight as it did whenever the pump was turned off. With a constant temperature, the mud maintaned a more constant viscosity.

Viscosity affected both the mud's carrying capacity and the pump's discharge pressure.

By switching from an 8 hour run period to around the clock experimentation, the fitting would be expected to erode in one third the number of days. But if the fitting were to wear out during the middle of the night, all the mud would be lost from the system and the exact end of the run time would not be known. To eliminate this uncertainty, it was decided to run all the fittings on a predetermined length of time rather than running until the fitting wore through. This normalized the run times so that all the individual wear patterns and weight changes could be compared to each other. A run time of 90 hours was chosen because that was the elapsed time when the pump motor burned out on the cast short radius ell.

Recalibrate the scale

One serious problem that developed after Run #2 was the discovery that the AccuWeight scale was badly out of calibration. The erroneous weighings indicated that 48.6 percent change in weight occured after a 67 hour run time. This could not be possible since most of the weight of each fitting was in the 2 flanges. The scale was recalibrated before any more fittings were tested. As a safeguard, all fittings were preweighed using a Toledo scale. After the AccuWeight scale was recalibrated, both scales agreed on

all fitting weights.

Valve replacement

One other noteworthy change was made on the flow loop system. A butterfly valve, located in the return leg, was replaced with a 2 inch ball valve. This proved to be a futile effort since this valve eroded worse than the butterfly valve. The ball valve was left fully open throughout the entire experiment but the brass housing eroded and the stainless steel ball remained intact.

CHAPTER SIX

RESULTS

6.1 Erosion Criteria

6.1.1 The Criteria

Three criteria were used in evaluating the erosion resistance of the pipe ells: 1) erosion pattern, 2) weight loss divided by exposed surface area, and 3) percent weight loss. Erosion pattern was illustrated with plots of the ultrasonic thickness test data before and after running in the flow loop. Weight loss per surface area is the change in fitting weight divided by the inside surface area of the fitting, expressed in pounds per square inch. And percent weight loss is simply the calculated percent change in fitting weight.

Table 4 is a summary of the test results and the experimental flow loop data for all the fittings. The Appendix containes a detailed listing of all the experimental data.

6.1.2 Erosion Pattern

The "BEFORE" and "AFTER" thicknesses were plotted against the distance along the fitting (from the upstream to the downstream positions). BEFORE thicknesses appear as a bold line while AFTER thicknesses appear as a thin line

and have symbols at each data point. The different symbols correspond to 3 different rows of ultrasonic thickness measurements: top, middle, and bottom. The 3 rows give a good picture of the erosion pattern and indicate whether the erosion was uniform over the fitting surface or if channeling erosion predominated. All fittings were mounted in the flow loop in such a way that the fluid flowed in a horizontal plane. They were all thickness tested along their center lines as well as along lines 1/2 inch above and 1/2 inch below their center lines. The words "TOP" signify the row that was above the center line and "BOTTOM" signifies the row below the center line. The symbol for the top row is a "Y", the center row is a "X", and the bottom row is a "+".

Each fitting was ultrasonically tested on both the outside and inside radii of curvature. Correspondingly, there are 6 plots for each fitting; 1 plot for each row and 3 rows per side. One exception to this was the short radius ell. Only the center line was tested on the inside radius. This fitting was run early in the experimental process and, at that time, it was felt that 3 rows per side were unnecessary.

On a few plots the AFTER line appears above the BEFORE line. This does not mean that the wall thickness increased as a result of running the flow test. It was actually caused by one of the routines used by the Benson computer

struck the fitting in the flow loop experiment. This made the above equation undefined and, therefore, unusable for this experiment. This problem prompted the use of the weight loss criteria were all the variables were known to a high accuracy and were easily obtainable.

Erosion pattern could not account for material loss over the entire eroded surface. The ultrasonic thickness readings could not be made closer than 1/2 inch to any flange face. Any erosion near the flanges would not be accounted for in the plots. Weight change per exposed surface area and percent weight change take into account erosion over the fitting's entire inside surface. Dividing weight change by inside surface area normalizes the losses of each fitting so they can to be compared directly.

6.1.4 Evaluation Using All Criteria

It is important to realize that the smallest percent weight loss does not necessarily indicate the highest erosion resistance. If erosion occurs in only a small, concentrated area, the fitting will experience a small weight loss. If this concentrated erosion were allowed to continue until a hole developed, the fitting would fail, yet only a small amount of material would have been lost.

Fitting weight that is not subjected to the erosive stream (flange weight) has the effect of artificially holding percent weight change low. If a fitting loses a

After closer inspection, it was apparent that the weldment material stuck out into the slurry flow and altered the flow pattern. The swirling flow eroded the pipe in a small, concentrated area. Further downstream, the pipe wall thickness appeared uniform. As will be mentioned in the next section, smooth welded connections are recommended to prevent this type of point erosion. It is interesting to note that the weldment material was not worn smooth by the erosive slurry.

6.3 Valves in the Flow Line

Several valves failed during this experiment. The butterfly valves eroded very quickly as did a 2 inch ball valve. The ball valve did not have an opening as large as the inside diameter of the pipe. In the butterfly valve, the pipe wall eroded right at the junction where the valve pivot and the pipe wall met. The only valve that remained intact was the a 6 inch butterfly located at the bottom of the mud tank where the fluid velocity was low and flow path was undisturbed. These findings indicate that restrictions and disturbances in the flow path tend to promote erosion at or near the disturbance. It is recommended that all valves be full opening and of the same size as the vent line. The valve's passage way should be as smooth as possible so as not to alter the flow path. The valve housing should be made of a material as hard or harder than the line pipe.

6.4 Fitting Evaluations

6.4.1 Welded Fitting Performances

The welded fittings were tested in the flow loop the same way as the cast fittings. But, because of the many problems encountered with initially setting up the equipment, the experimental variables could never be held constant. Several data were not recorded correctly or were not recorded at all. The welded fitting runs were used mainly for working out problems in the experimental procedure.

The results of the welded short radius ell and the welded plugged tee are given in the back of the Appendix. If the plots are compared with those of the cast fitting counterparts, no correlations can be drawn. Wide variations in erosion pattern are expected because the weldment material alters the flow pattern. Even between 2 of the same type of welded members, erosion patterns are expected to vary widely. For these reasons, the welded fittings were not considered in the evaluations. To reduce the effects of an altered flow path, it is suggested that all welded connections be made as smooth as possible.

6.4.2 Cast Fitting Performances

Based on the 3 erosion criteria, fittings were analysed and ranked for their resistance to erosion, from most resistant to least resistant.

1st - short radius ell

2nd - plugged tee

3rd - long radius ell

4th - Vortice-Ell

Plots of the erosion patterns are presented in this chapter and are followed by analyses of the fitting's overall performance.

The flow loop data shows that the long radius ell had the lowest pressure drop of all the fittings. Pressure drop in the vent line is an important consideration because the pressure is transfered to the formation in the form of backpressure. The short radius ell also created a small pressure drop. The plugged tee and the Vortice-Ell both caused substantially higher pressure drops. The fittings were evaluated on the basis of erosion resistance and not on pressure drop, so the short radius ell is still the preferred fitting.

From careful examination of the data summary table and erosion patterns, it is apparent that there is no direct correlation between the amount of erosion and sand content. The grain size distribution plots did not correlate with erosion either. This finding suggests that complex relationships are at work and further supports the use of erosion pattern and weight loss as the evaluation criteria.

6.4.3 Short Radius Ell

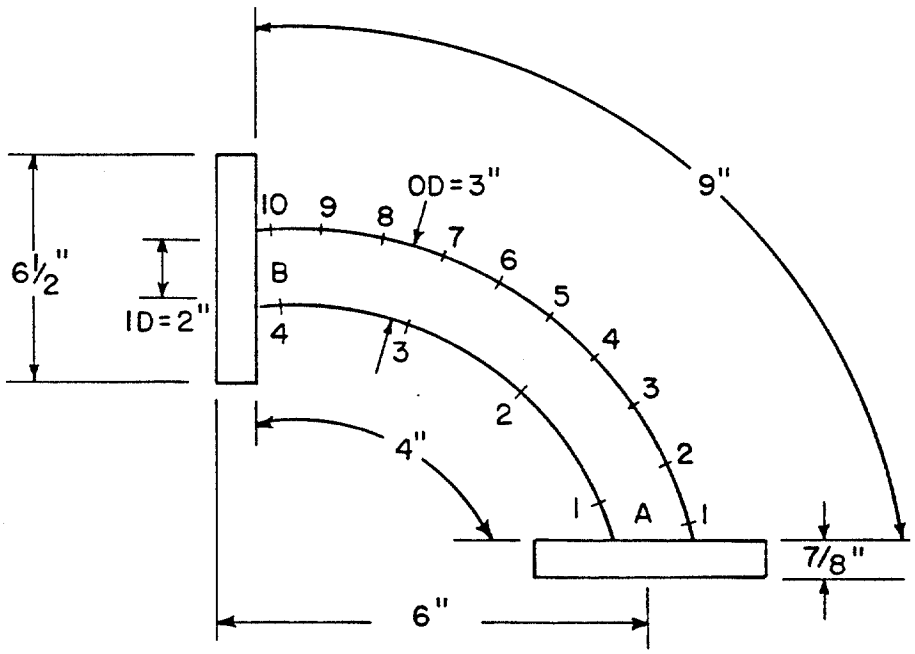

Figure 20. Short radius ell geometry.

SHORT RADIUS ELL

Erosion Patterns

INSIDE RADIUS

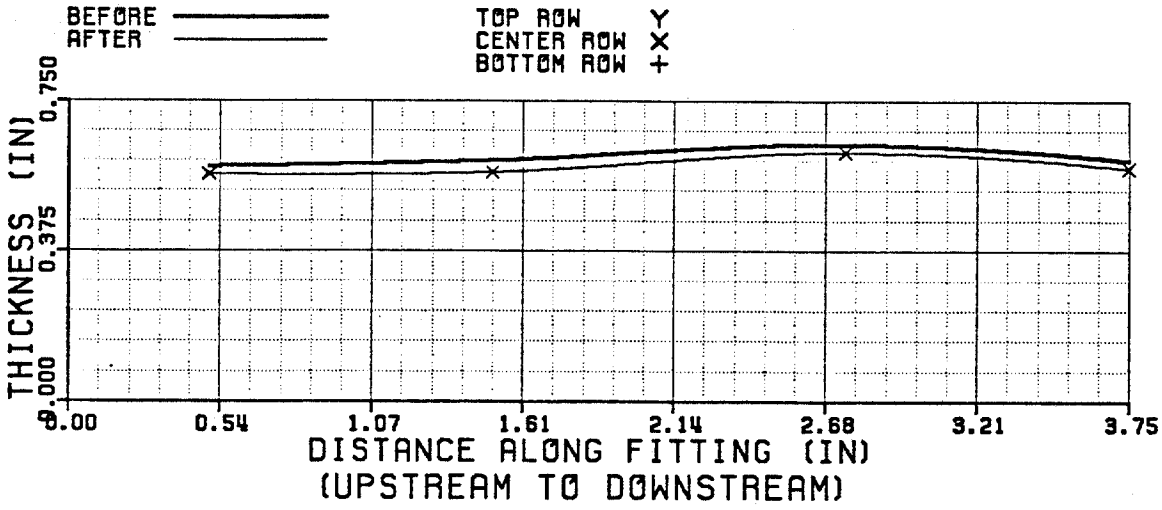

CAST SHORT RADIUS ELL
INSIDE (A TO B)

OUTSIDE RADIUS

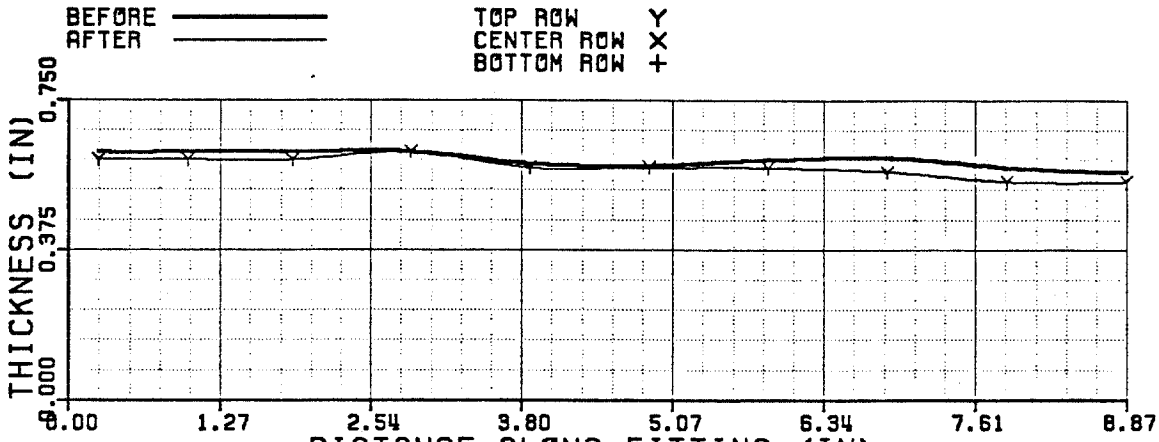

CAST SHORT RADIUS ELL
OUTSIDE (A TO B)

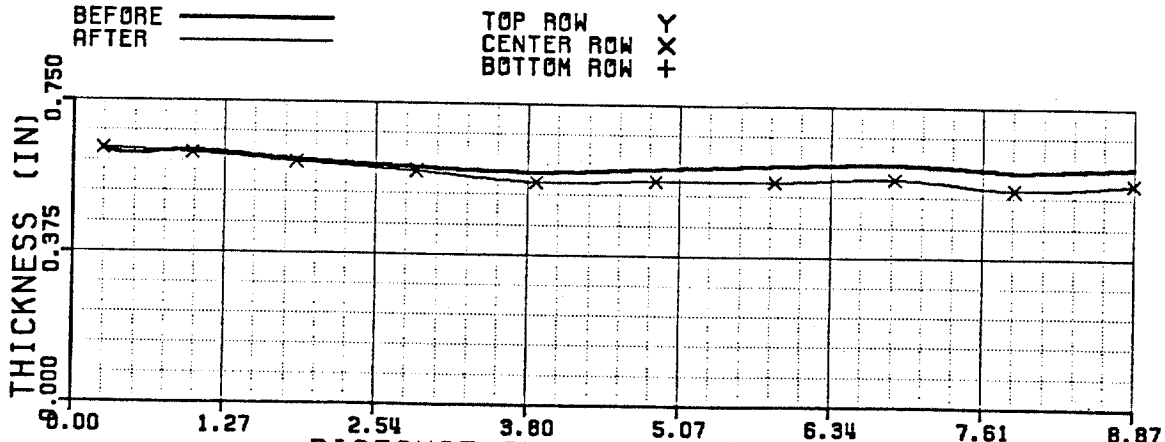

CAST SHORT RADIUS ELL
OUTSIDE (A TO B)

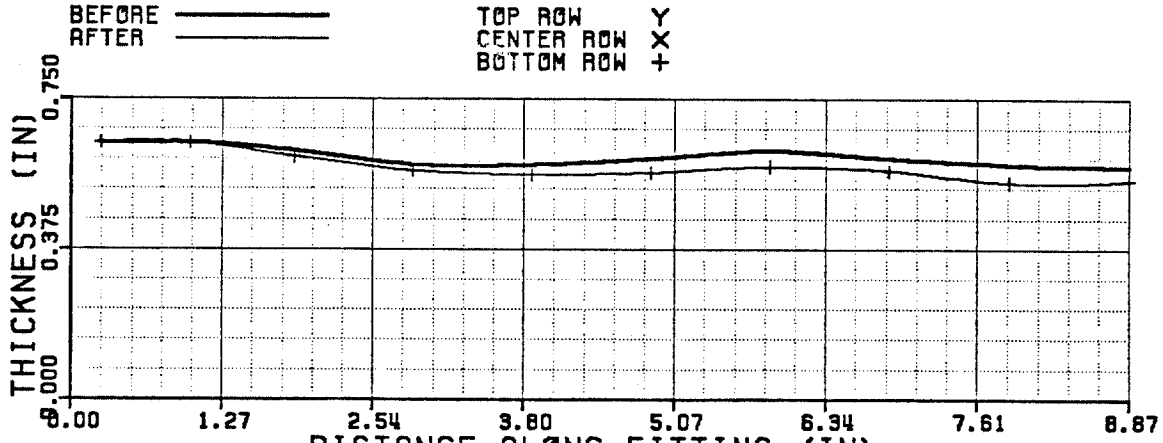

CAST SHORT RADIUS ELL
OUTSIDE (A TO B)

The short radius ell showed the smallest percent weight loss, 2.45%, and the smallest weight loss per exposed area, Ø.Ø136 psi. Its value of maximum pipe wall thickness change, Ø.Ø56 inches, was also the lowest of the fittings. All of these figures and the erosion pattern suggest that a very small amount of material was removed.

The small amount of erosion that did occur was all uniform in pattern. This suggests that the whole fitting would uniformly wear thin and fail only after a long flow time. The lack of any concentrated erosion was the primary reason for ranking the short radius ell number 1 in erosion resistance.

The inside radius plot indicates the minimal amount of erosion that took place. The first point (at the inlet) corresponds to a thickness change equal to Ø.Ø2 inches and the other points represents about the same amount. Ultrasonic tests were run only at the centerline on the inside radius. Based on the erosion pattern of the long radius ell, it was assumed that top and bottom rows would have exhibited the same erosion patterns as the center row.

The outside radius plots also indicate small amounts of material loss. The pattern shows no areas of concentrated erosion. A minimum amount of erosion occured at the inlet and increased continuously from the inlet to the outlet. The maximum thickness change at the exit,

Ø.Ø56 inches, was still very small in magnitude.

The short radius ell received the highest ranking for erosion resistance because it was not limited by any criteria. It was felt that the short radius ell would provide a longer service time than all the other fittings.

6.4.4 Plugged Tee

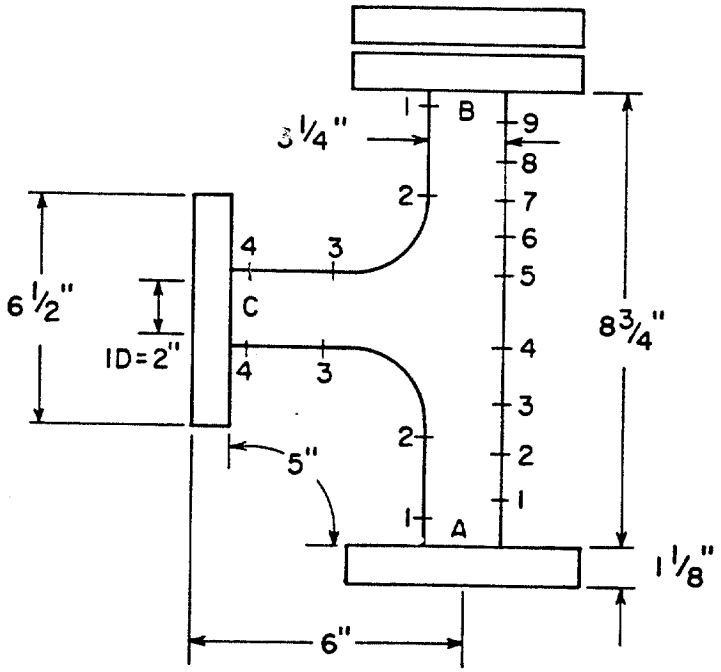

Figure 21. Plugged tee geometry.

PLUGGED TEE

Erosion Patterns

INSIDE RADIUS

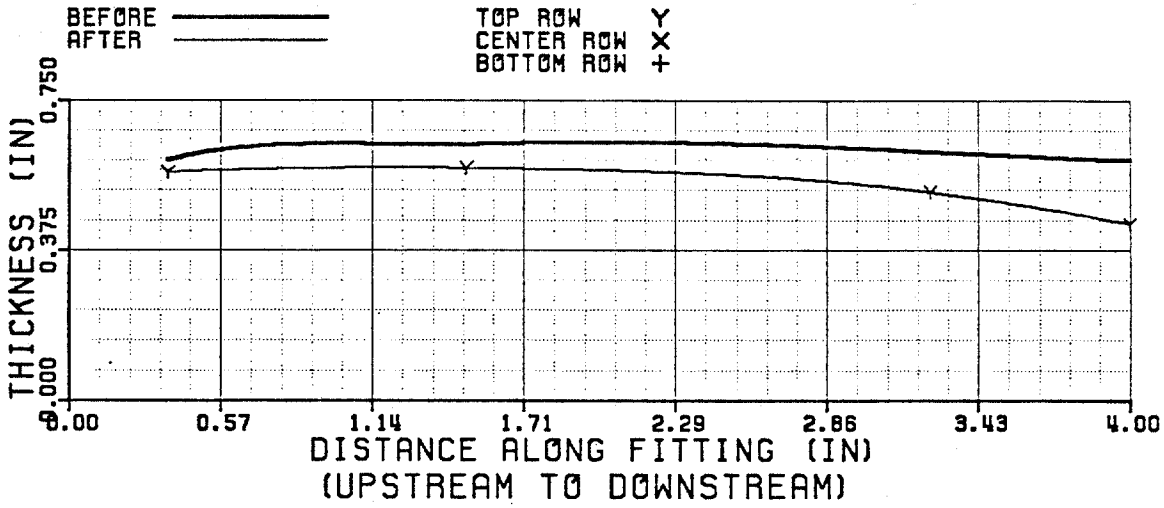

CAST PLUGGED TEE
INSIDE (A TO C)

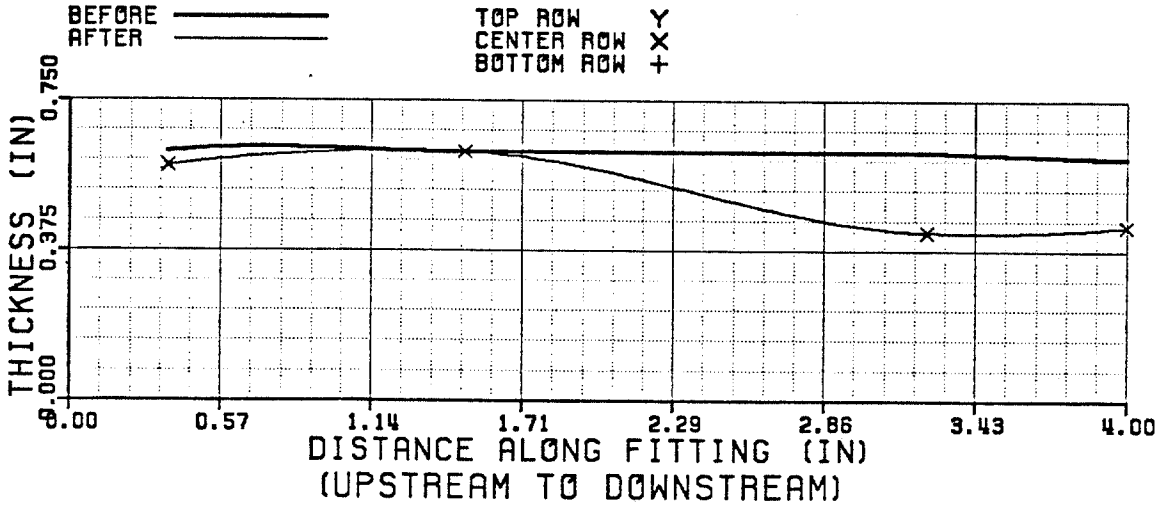

CAST PLUGGED TEE
INSIDE (A TO C)

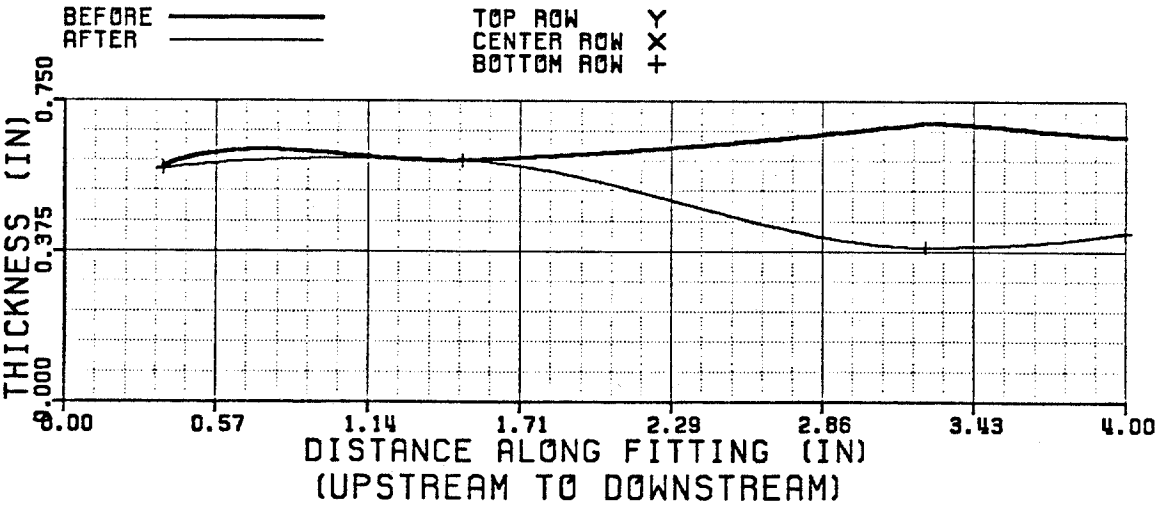

CAST PLUGGED TEE
INSIDE (A TO C)

INSIDE RADIUS

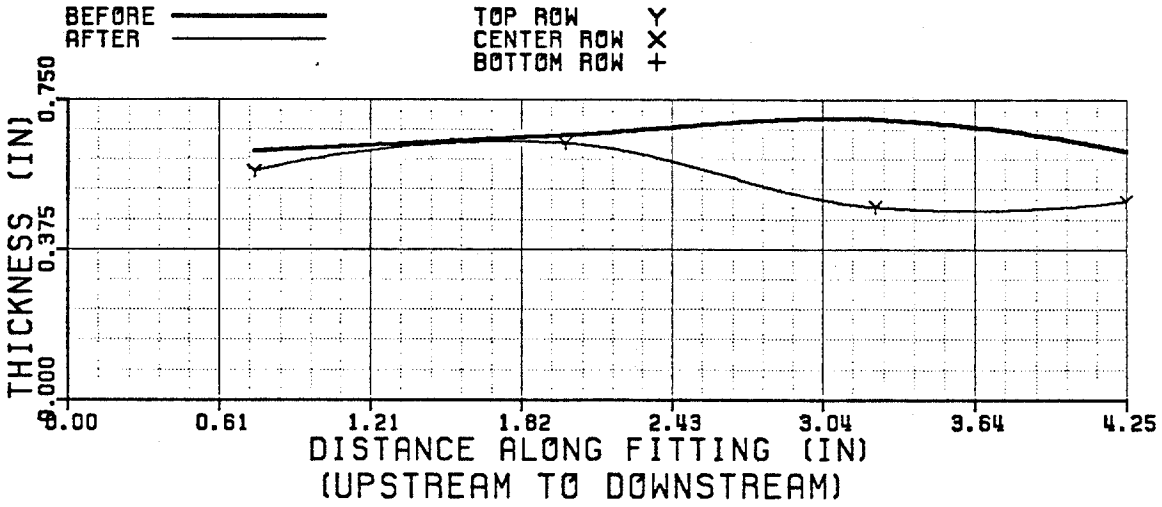

CAST PLUGGED TEE
INSIDE (B TO C)

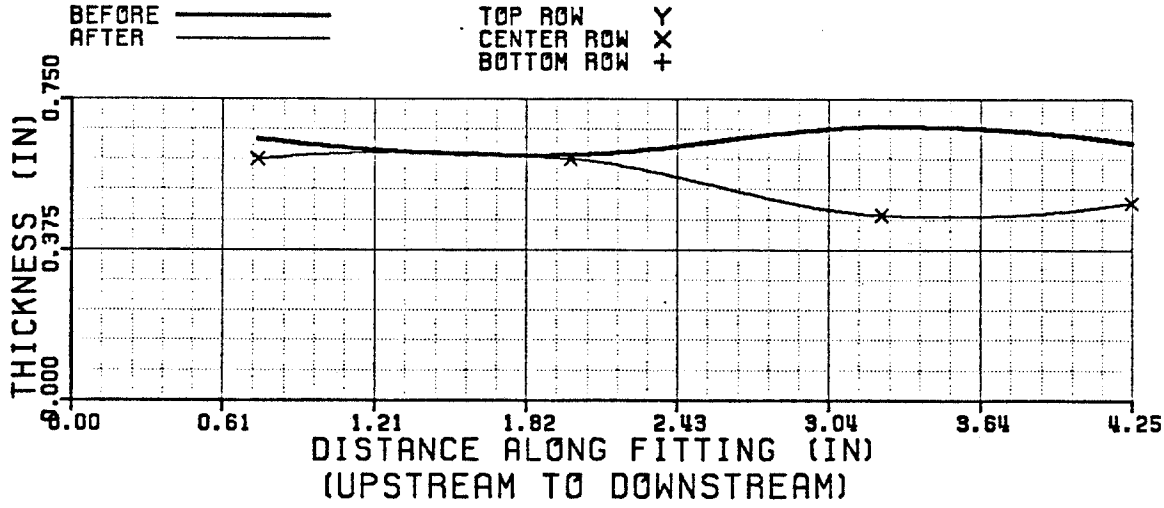

CAST PLUGGED TEE
INSIDE (B TO C)

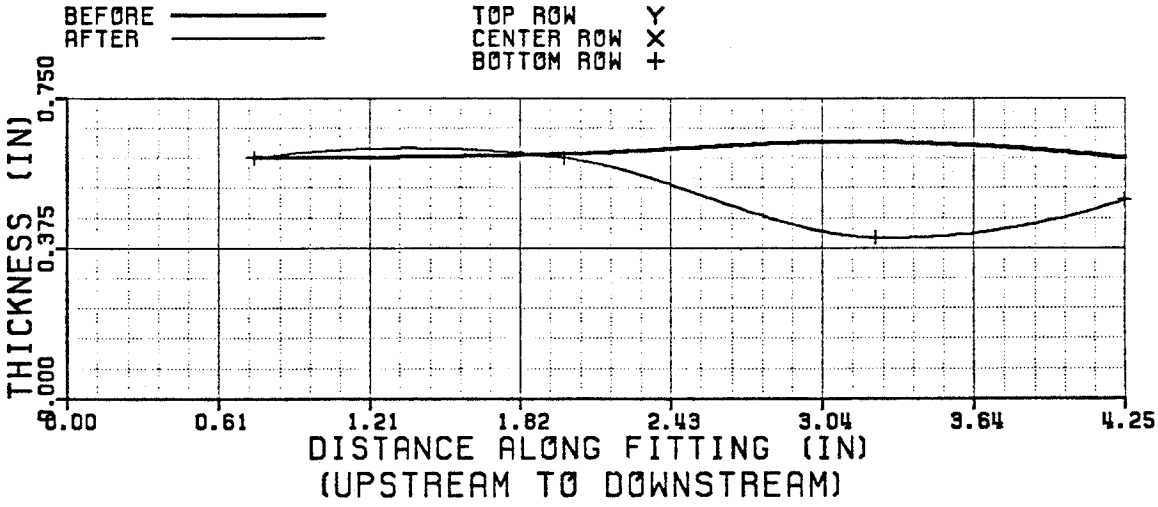

CAST PLUGGED TEE
INSIDE (B TO C)

OUTSIDE RADIUS

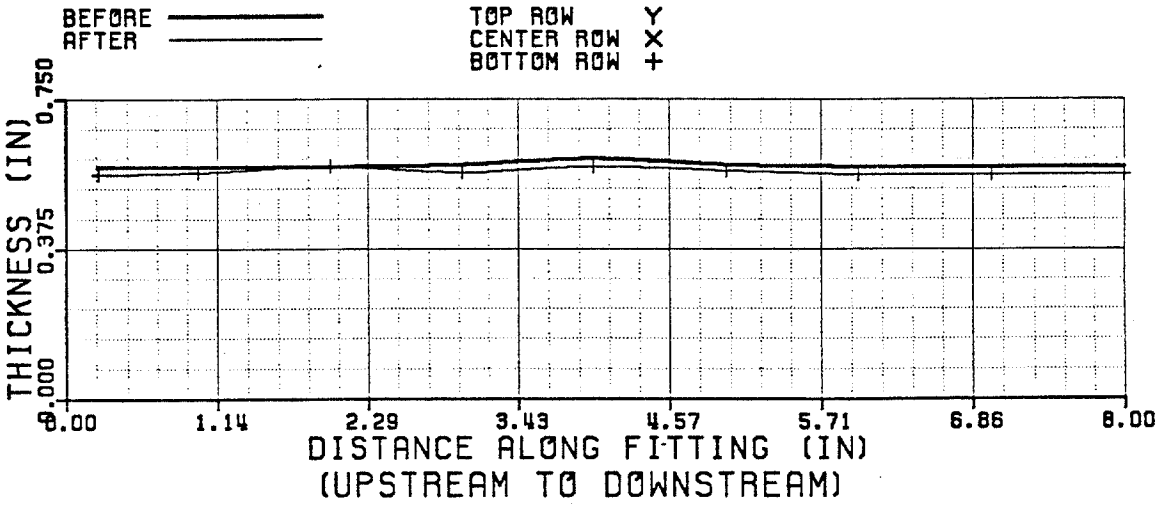

CAST PLUGGED TEE
OUTSIDE (A TO B)

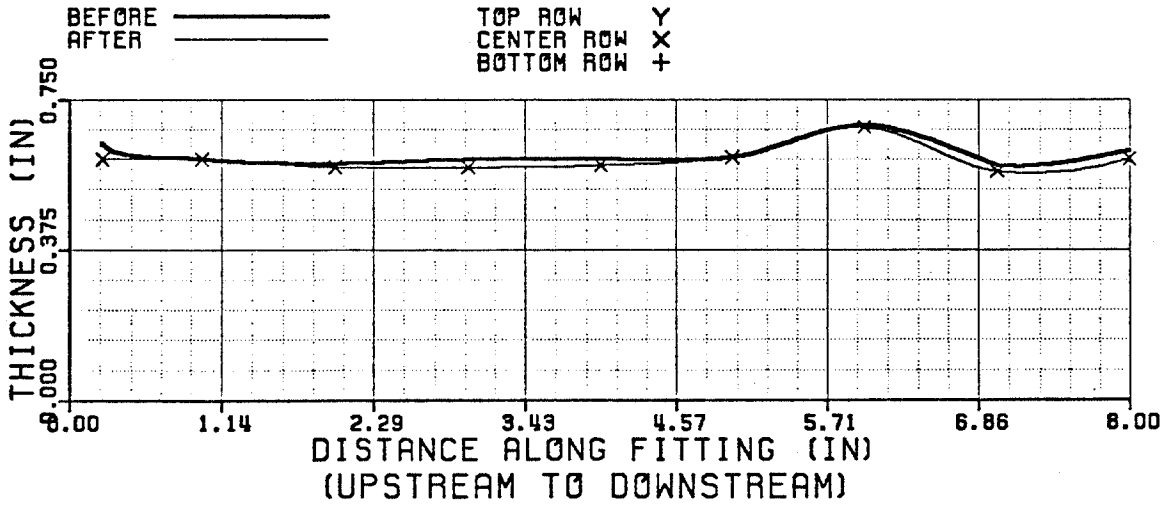

CAST PLUGGED TEE
OUTSIDE (A TO B)

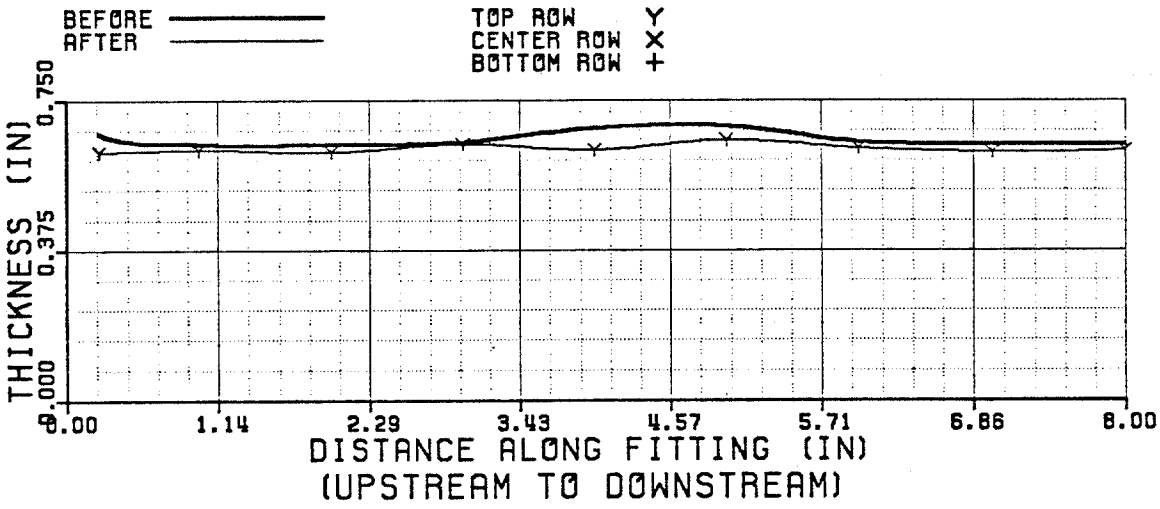

CAST PLUGGED TEE
OUTSIDE (A TO B)

This fitting lost a considerable amount of material, as evidenced by the weight loss per surface area figure. The plugged tee has 3 flanges, 1 more than the other fittings, so the percent change in weight was artificially held low by the third flange. The plugged tee lost Ø.Ø222 pounds per square inch, yet only showed a 3.66 percent change in weight. This is a relatively large amount of material loss when compared with the weight losses of the other fittings.

The plugged tee has 2 inside surfaces and 1 outside surface, as shown in the drawing. The straight section from A to B underwent only a slight amount of uniform erosion. Since there were no areas of concentrated erosion, this portion of the plugged tee is not expected to be a limitation in the useful life of this fitting.

The A to C inside radius, from the inlet to the exit, displays considerable erosion at the exit. Almost no erosion occured at the inlet, but thickness change at the exit was as large as Ø.31 inches. This is a very large amount of material loss and was the main reason for ranking the plugged tee below the short radius ell.

The dead-end section, B to C, shows a similar wear pattern as that of section A to C. Very little erosion occured at the inlet and a great deal of material was lost at the exit. This data also suggests that the plugged tee is limited by erosion at its exit. Combined with the plots

from A to C, this data shows that erosion occurs uniformly around the exit and not preferentially to one side.

The erosion patterns of sections A-C and B-C are very similar yet there is a major difference between the curves. The first 2 data points on the A to C curve lie at the inlet of the plugged tee. The first 2 points on the B to C curve lie in the dead-end portion of the plugged tee. The B to C curve shows that some erosion did occur in the dead-end segment. This was a surprising result since the fluid inside the dead-end section was thought to be "stagnant". That is often the reasoning given for running plugged tees: that the dead-ended area catches some of the fluid, holds it in place, and allows the incoming fluid to strike the stagnant fluid. This theory cannot be accurate since erosion occured in the dead-end area. The erosive stream entered the dead-end section and was forced to turn around after striking the blind flange. It also appears that erosion was greatest near the blind flange and decreased in the downstream direction. This suggests that a swirling type of fluid flow causes erosion in the dead-end.

The erosion pattern of this fitting can be called concentrated because only a small portion of the fitting eroded to an appreciable extent. The uniform erosion in other areas of the fitting was negligible compared with the erosion at the exit. The concentrated erosion pattern was the limiting factor for the plugged tee.

6.4.5 Long Radius Ell

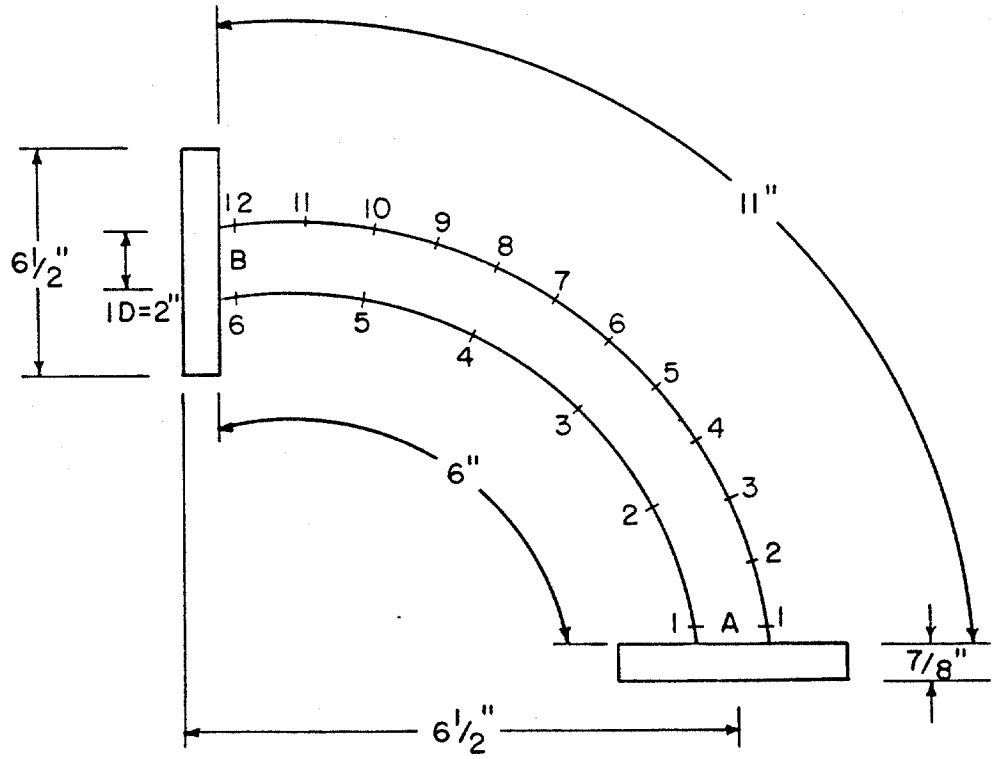

Figure 22. Long radius ell geometry.

LONG RADIUS ELL

Erosion Patterns

INSIDE RADIUS

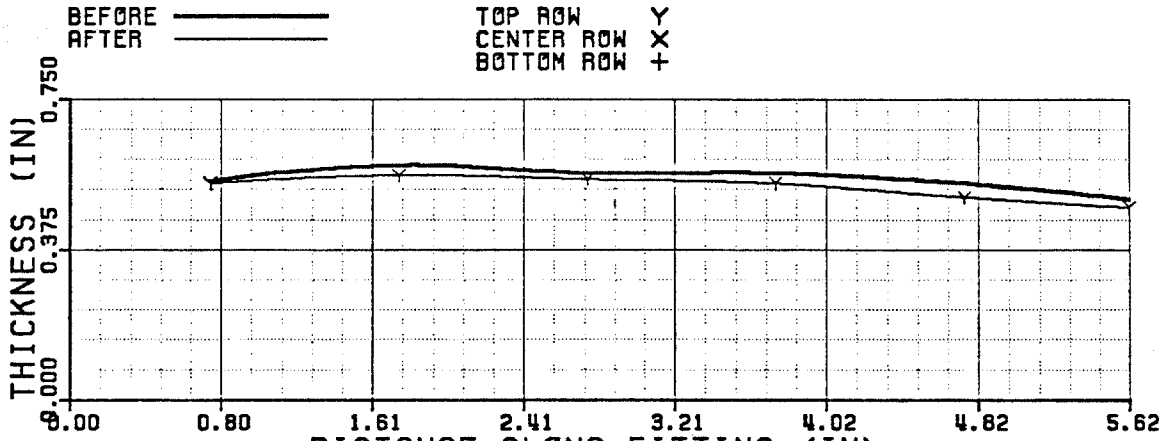

CAST LONG RADIUS ELL
INSIDE (A TO B)

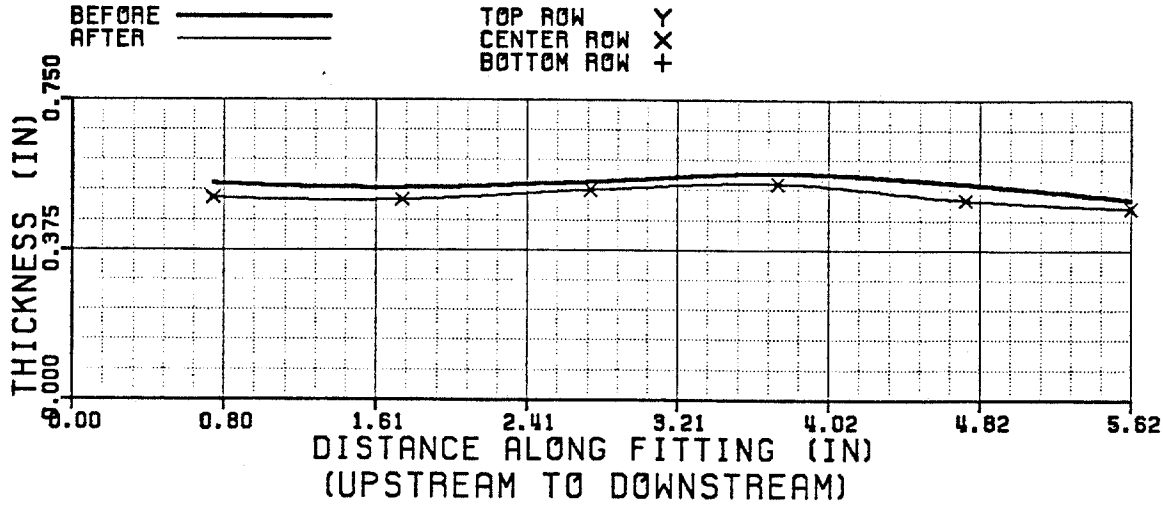

CAST LONG RADIUS ELL
INSIDE (A TO B)

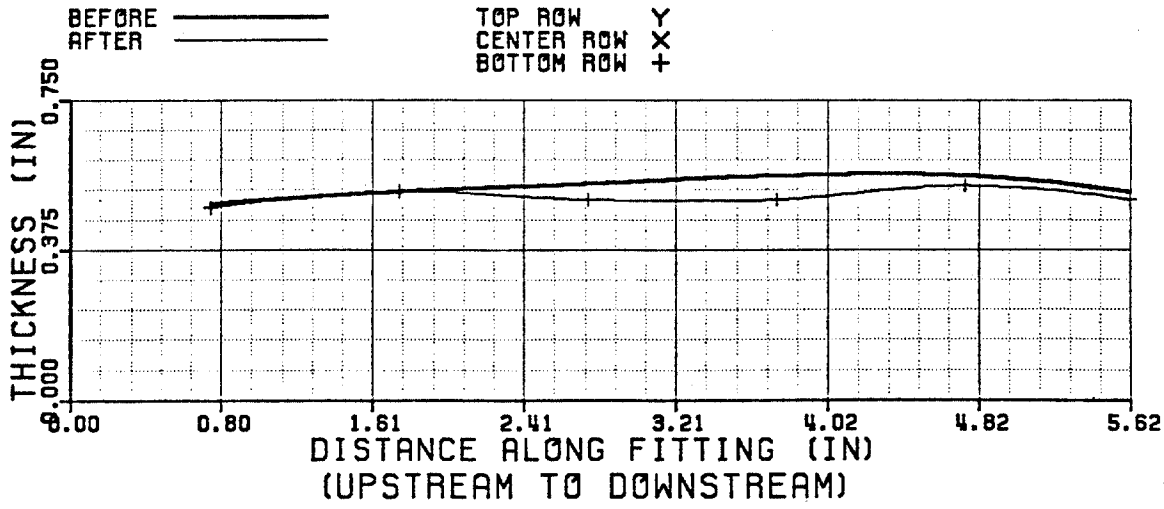

CAST LONG RADIUS ELL
INSIDE (A TO B)

OUTSIDE RADIUS

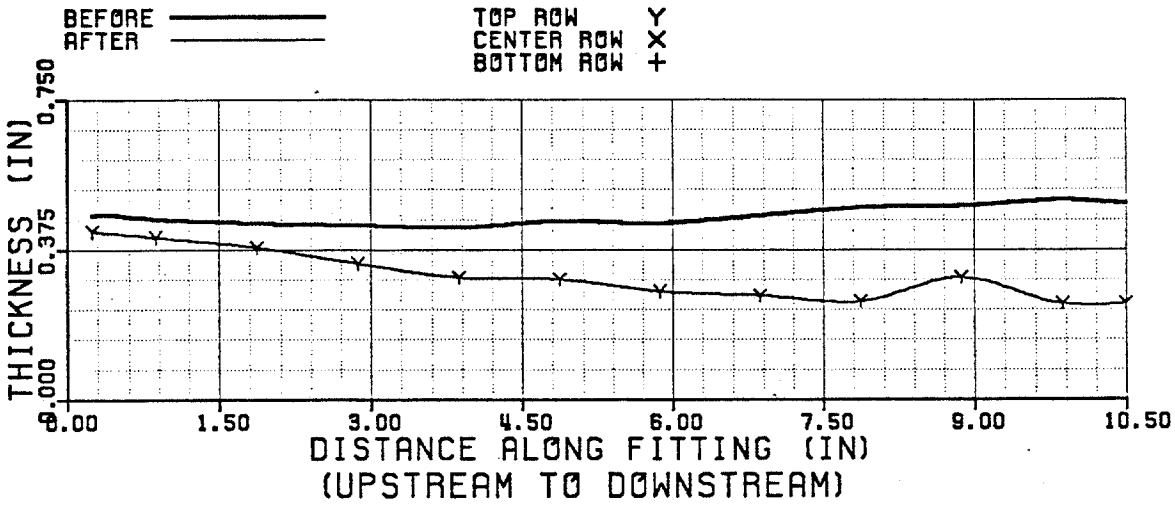

CAST LONG RADIUS ELL
OUTSIDE (A TO B)

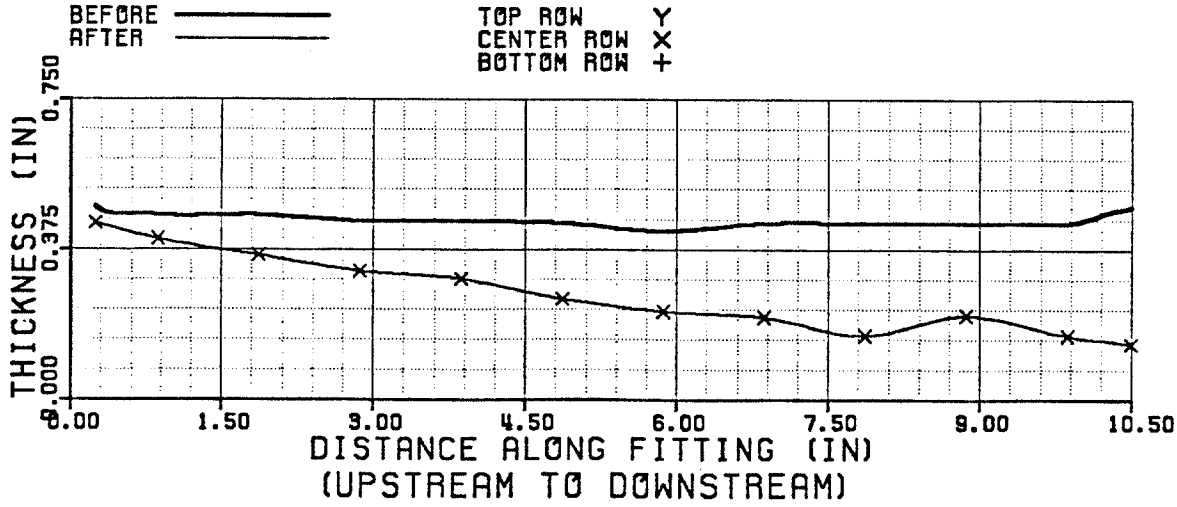

CAST LONG RADIUS ELL
OUTSIDE (A TO B)

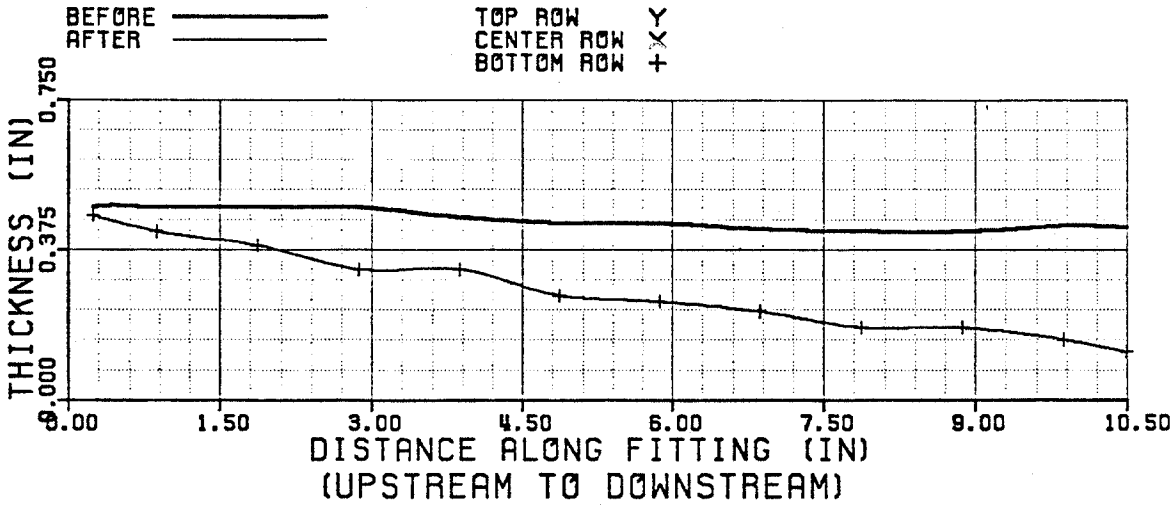

CAST LONG RADIUS ELL
OUTSIDE (A TO B)

This fitting had the highest value of percent weight loss, 6.46%, and the highest value of weight loss per exposed surface area, Ø.Ø258 pounds per square inch. It also had the second largest thickness change value, Ø.338 inches. These figures indicate that a large amount of material was removed.

The erosion patterns of both the inside and outside surfaces were very similar to those of the short radius ell. The inside radius showed a very small amount of uniform erosion from the inlet to the exit with no trend of increasing erosion and no areas of concentrated erosion.

The outside radius showed a small amount of erosion at the inlet which gradually increased from the upstream to the downstream positions. Since the long radius ell has a greater curvilinear length than the short radius ell, it experienced a greater total thickness change. The large amount of material loss is illustrated by the BEFORE and AFTER curves, especially near the exit.

This fitting received such a low ranking (third) primarily because of the large amount material loss. Erosion pattern was not considered the limiting criterion because it was so similar to that of the short radius ell.

6.4.6 Vortice-Ell

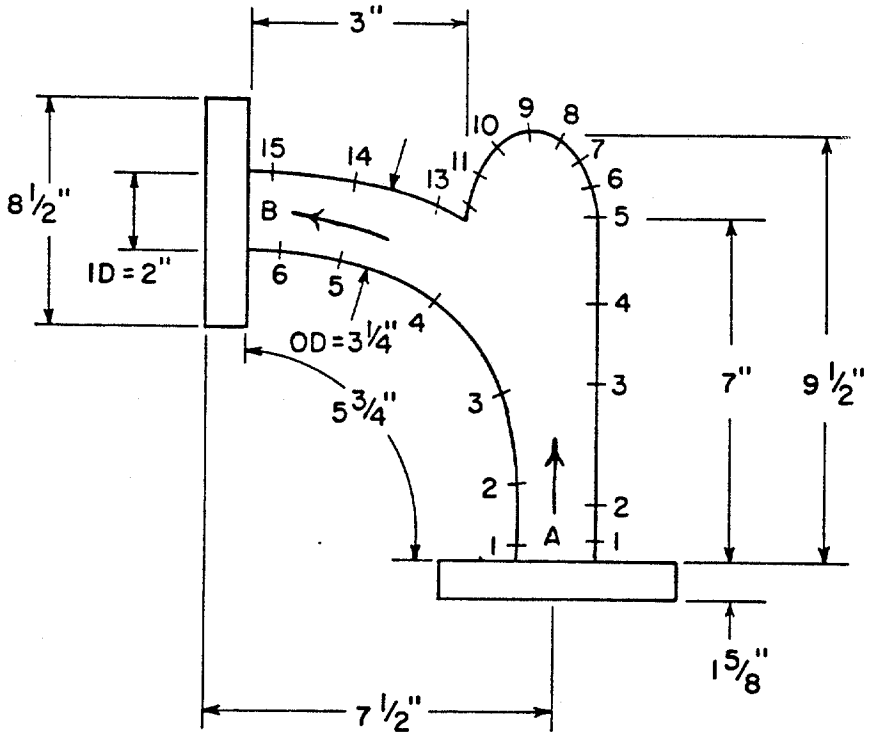

Figure 23. Vortice-Ell geometry.

VORTICE-ELL

Erosion Patterns

INSIDE RADIUS

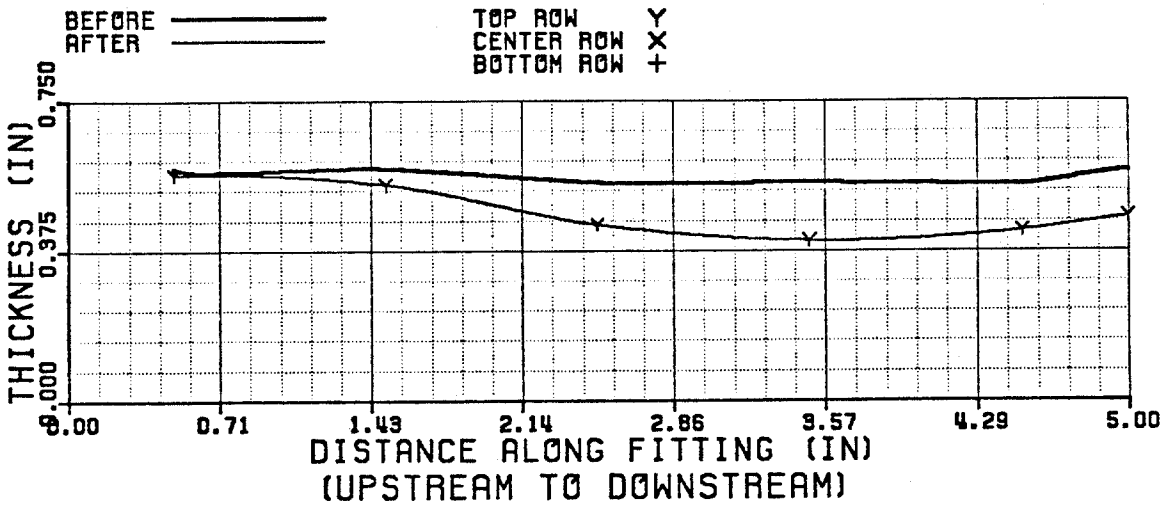

CAST VORTICE ELL
INSIDE (A TO B)

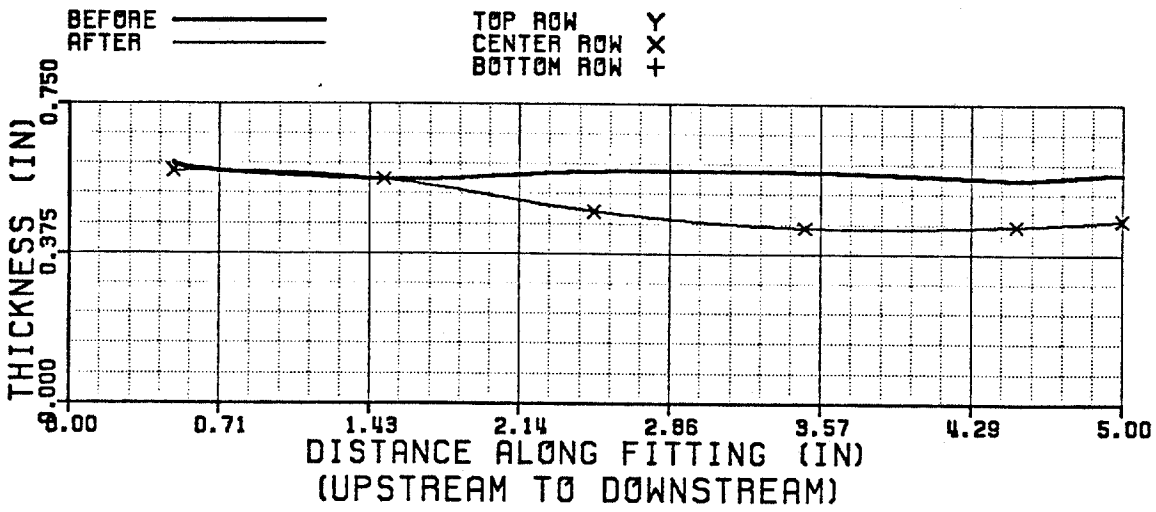

CAST VORTICE ELL
INSIDE (A TO B)

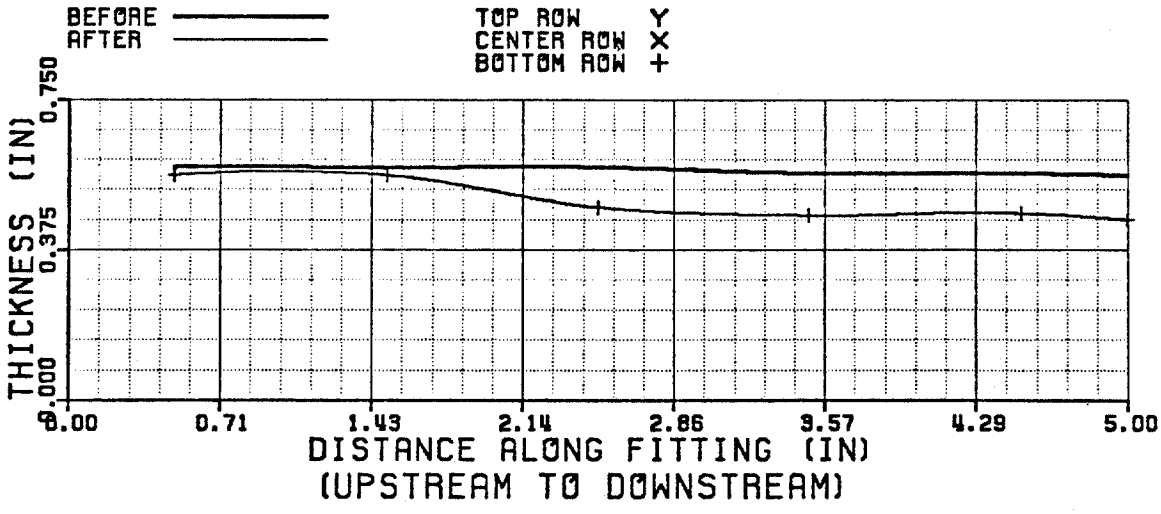

CAST VORTICE ELL
INSIDE (A TO B)

OUTSIDE RADIUS

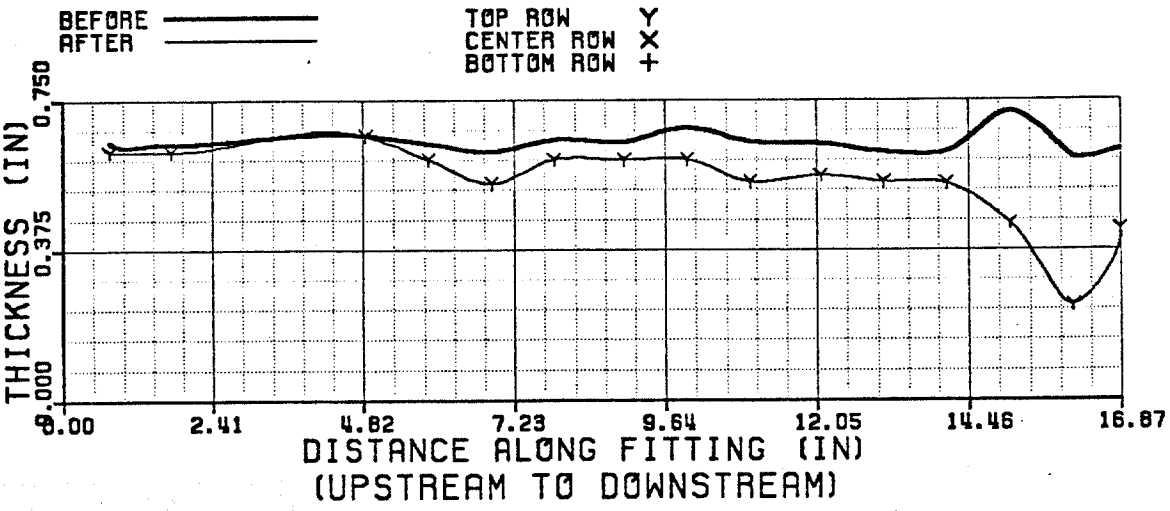

CAST VORTICE ELL
OUTSIDE (A TO B)

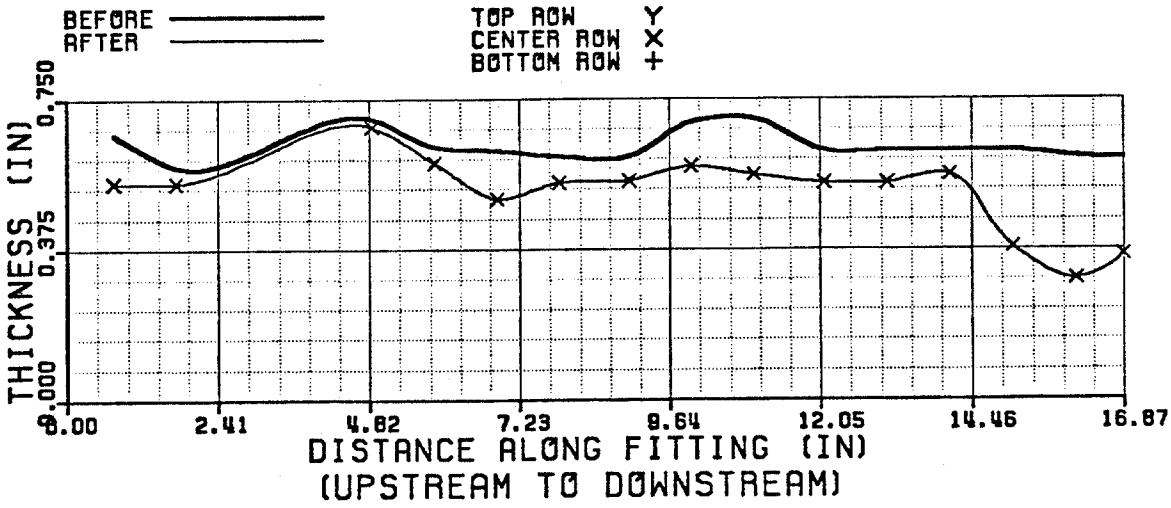

CAST VORTICE ELL
OUTSIDE (A TO B)

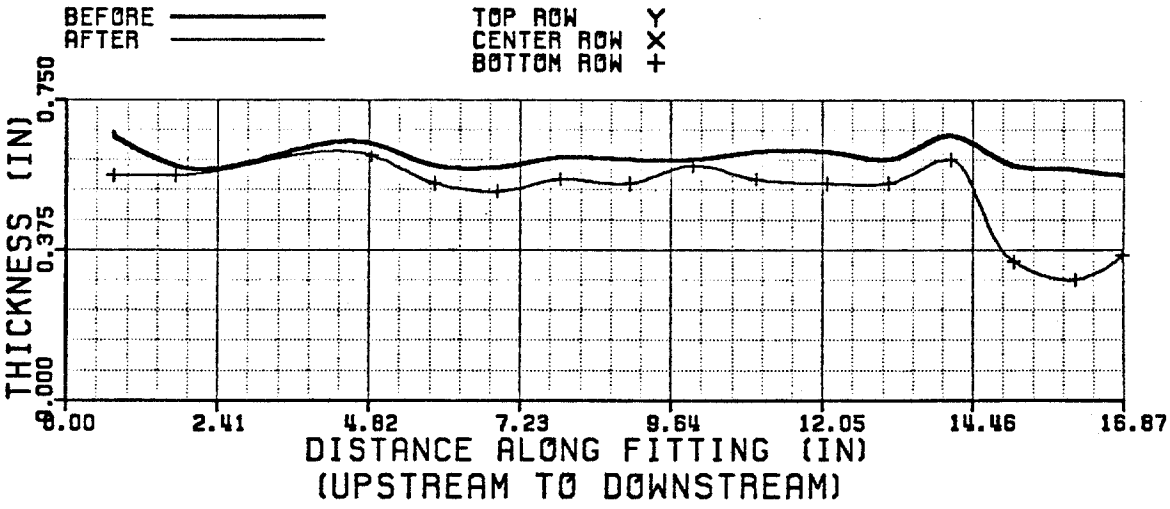

CAST VORTICE ELL
OUTSIDE (A TO B)

The Vortice-Ell had the second largest weight loss per surface area, Ø.Ø222 pounds per square inch. The percent change in weight calculated to be a small number, 3.Ø6, but this value was influenced by the large flange weight. The Vortice-Ell has only 2 flanges but each were rated at 15ØØ psi and measured 1 5/8 inches in thickness and 8 1/2 inches in diameter. The flanges for all the other fittings were rated at only 3ØØ psi and measured 5/8 inches in thickness and 6 1/2 inches in diameter. The initial weight of the Vortice-Ell was 61.85 pounds whereas the next heaviest member, the plugged tee, only weighed 42.86 pounds. The Vortice-Ell flanges added much more weight than the other flanges and, thus, held the percent weight change low.

All 3 plots of the inside radius showed the same erosion pattern: little erosion near the inlet and a considerable amount of erosion further downstream. By examining the Vortice-Ell drawing, it can be seen that the major area of erosion occured opposite the "vortex chamber" (the bulb) and at points downstream. The plots indicate a uniform erosion pattern downstream of the vortex chamber and negligible erosion upstream.

The sketch of the Vortice-Ell illustrates how the outside radius has 3 distinct sections: the straight section going from the inlet to where the vortex chamber starts to curve, the vortex chamber, and the curved section just downstream of the bulb. Each of these sections had

its own distinct erosion pattern.

The straight section includes all data points up to and including point number 4. This surface exhibited a small amount of uniform erosion. There appeared to be some concentrated erosion at the inlet, but this was not supported by measurements on the inside radius. Erosion was minimal along the straight section and increasesd to a considerable magnitude at the vortex chamber.

The erosion pattern was uniform throughout the vortex chamber. The magnitude of erosion and the lack of concentrated erosion agreed well with the pattern from the short radius ell where the target surface also curved sharply. The vortex chamber erosion pattern differed from that of the long radius ell in that erosion did not increase in a steady fashion from upstream to downstream. Neither the straight section nor the vortex chamber limited the usefulness of this fitting.

The last section, from the end of the bulb to the flange face, proved to be the limiting section on the Vortice-Ell. Each plot showed a large amount of concentrated erosion just after the vortex chamber. One point had the largest thickness change among all the fittings; Ø.36 inches. It appears that the middle point along this curved section, point number 14, always exhibited the maximum amount of erosion. This was possibly due to a swirling flow pattern similar to that in the

plugged tee. It is believed that this concentrated erosion would continue until the fitting failed. For this reason, and the large amount of material loss, the Vortice-Ell received the lowest ranking of all the fittings.

It was learned, only after the experiments were completed, that the Vortice-Ell was designed to change the flow stream direction from horizontal to vertical. Unfortunately, it was not tested in this arrangement. One of the representatives of the HammerTek Corporation explained that the force of gravity on the abrasive had an important affect on the performance of the Vortice-Ell. In commercial applications, it has proven very effective in reducing erosion failures of pneumatic-transportation systems. This study was the first time the fitting was tested with a liquid for the carrying fluid.

CHAPTER SEVEN

CONCLUSIONS AND RECOMMENDATIONS

The conclusions drawn from this study are:

1. The laboratory type erosion experiments used by previous investigators were not useful in testing pipe bends.

2. The erosion models could not be applied to the flow loop experiment used in this study.

3. The straight sections of pipe in the flow loop used in this study showed no appreciable amounts of erosion.

4. Valves that created the least amount of disturbance in the flow path gave the longest service lives.

5. The welded fittings eroded in erratic patterns and showed no correlation with the cast fittings.

6. Based on an analysis of the experimental data, the fittings were given the following ranking for erosion resistance (from most resistive to least resistive):

   a) short radius ell,

   b) plugged tee,

   c) long radius ell,

   d) Vortice-Ell.

7. The magnitude and pattern of erosion showed no direct correlations with sand concentration and grain size

distribution.

8. In relation to imparting backpressure on the formation, the long radius ell produced the lowest pressure drop, followed closely by the short radius ell, then the plugged tee, and, finally, the Vortice-Ell.

The recommendations resulting from this study are:

1. Diverter vent lines should be designed and installed as straight as possible.

2. If bends must be used, then short radius ells should be employed.

3. All welded connections, whether at fittings or in straight pipe, should be as smooth as possible.

4. Valves should be full opening to the same diameter as the vent line and should cause a minimum of disturbances in the flow pattern.

An additional recommendation is that further study into the erosion of diverter vent lines is needed. The continued study should include experimental work using air or some other gas as the carrying fluid.

LIST OF REFERENCES

Behrendt, A. 1970. Proc. Int. Conf. Rain Eros. Assoc. Phenomena, 3rd, RAE, England II, 797-820.

Bitter, J.G.A. 1963a. A study of erosion phenomena, Part I. Wear. 6:5-21.

Bitter, J.G.A. 1963b. A study of erosion phenomena, Part II. Wear. 6:169-90.

Eyre, T.S. and Dutta, K. 1975. Int. Mech. Engr. Conf. Piston Ring Scuffing. Paper C 74/75.

Eyre, T.S. 1979. Wear resistance of metals. Treatise On Material Science And Technology. 13:363-442.

Finnie, I. 1960. Erosion of surfaces by solid particles. Wear. 3:87-103.

Finnie, I., Wolak, J., and Y. Kabil. 1967. Erosion of metals by solid particles. Journal of Materials. 2:682-700.

Kruschov, M. N. 1957. Inst. Mech. Engr. Conf. Lub. Wear. 655.

Mason, J. S. and Mills, D. 1977. Int. Powder and Bulk Solids Handling and Proc. Conf., 2nd, Chicago, Illinois.

Neilson, J. H. and A. Gilchrist. 1968a. Erosion by a stream of solid particles. Wear. 2:111-22.

Neilson, J. H. and A. Gilchrist. 1968b. An experimental investigation into aspects of erosion in rocket motor tail nozzles. Wear. 2:123-43.

Paulson, J. 1985. Private communication.

Richardson, R. C. 1968. The wear of metals by relatively soft abrasives. Wear. 2:245-275.

Sage, W. and G. P. Tilly. 1969. The significance of particle size in sand erosion of small gas turbines. Aero J. 73:427-28.

Serpik, N. M. and M. M. Kantor. 1965. Frict. Wear Mach. 19:28

Sheldon, G. L. and I. Finnie. 1966. The mechanism of material removal in the erosive cutting of brittle materials. Transactions of the ASME. 393-400.

Tilly, G. P. 1969. Erosion caused by airborne particles. Wear. 14:63-79.

Tilly, G. P. 1973. A two stage mechanism of ductile erosion. Wear. 23:87-96.

Tilly, G. P. 1979. Erosion caused by impact of solid particles. Treatise on Materials Science and Technology. 13:287-319.

APPENDIX

EXPERIMENTAL DATA

The flow loop described in the chapter entitled EXPERIMENTAL APPARATUS was used to test 4 different cast fittings. The short radius ell was tested first, followed by the plugged tee, then the long radius ell, and, finally, the Vortice-Ell. This Appendix lists the data recorded while testing each fitting, including the dimensions of each fitting, their weights before and after testing, their pipe wall thicknesses before and after testing, the locations of the thickness measurement points, and the flow loop data. Flow loop data includes the following: flowline pressure, differential pressure across the fitting, temperatures upstream and downstream of the fitting, pump flowrate, sand content of the mud/sand slurry, sand sieve analysis, and mud density, viscosity, and yield point. The results of the welded fitting runs are presented at the end of this Appendix. The experimental data for these fittings are not provided since it was often incomplete or not very representative.

DATA COMMON TO ALL TEST RUNS

Drilling mud composition - mixture of Magobar bentonite clay (Magogel), caustic soda, and fresh water.

TABLE 5

NUMBER TWO BLASTING SAND INITIAL GRAIN SIZE DISTRIBUTION
SAMPLE NUMBER ONE

US sieve number	sieve opening (mm/in)	weight retained (gm)	weight %	cumulative weight %
10	2.000/0.0787	19.60	2.52	2.52
16	1.180/0.0469	119.46	15.37	17.89
30	0.590/0.0232	237.04	30.51	48.40
40	0.420/0.0165	200.01	25.74	74.14
50	0.297/0.0116	165.92	21.35	95.49
80	0.177/0.0070	34.35	4.42	99.91
100	0.149/0.0059	0.30	0.04	99.95
200	0.074/0.0029	0.26	0.03	99.98
tray	-	0.05	0.01	99.99
		766.99	100.00	

TABLE 6

NUMBER TWO BLASTING SAND INITIAL GRAIN SIZE DISTRIBUTION
SAMPLE NUMBER TWO

US sieve number	sieve opening (mm/in)	weight retained (gm)	weight %	cumulative weight %
10	2.000/0.0787	19.80	2.82	2.82
16	1.180/0.0469	96.28	13.73	16.55
30	0.590/0.0232	200.51	28.60	45.15
40	0.420/0.0165	185.37	26.44	71.59
50	0.297/0.0116	146.17	20.85	92.43
80	0.177/0.0070	52.30	7.46	99.89
100	0.149/0.0059	0.58	0.08	99.97
200	0.074/0.0029	0.13	0.02	99.99
tray	-	0.05	0.01	100.00
		701.19	100.00	

Figure 24 is a plot of the initial grain size distribution.

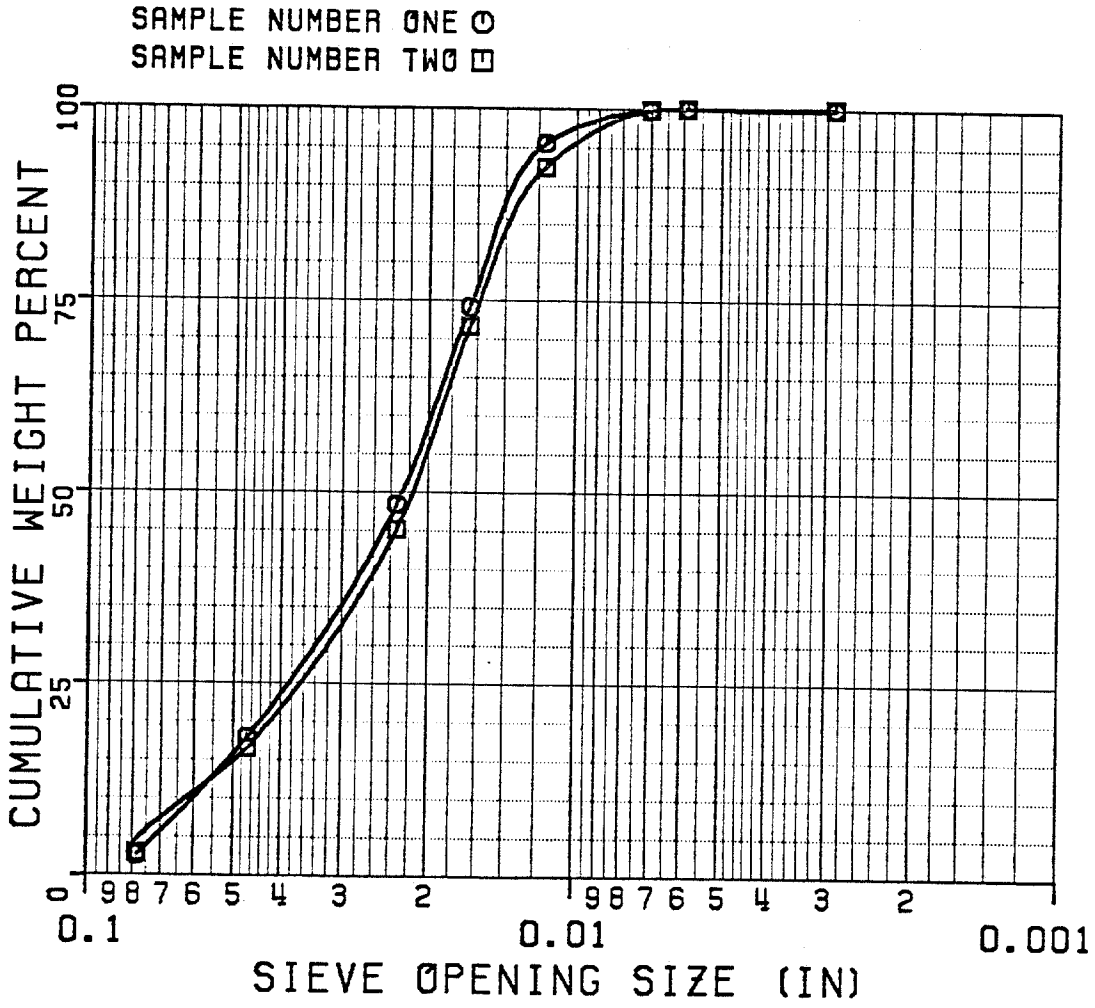

GRAIN SIZE DISTRIBUTION

Figure 24. Grain size distribution of the initial number 2 blasting sand.

EXPERIMENTAL DATA

SHORT RADIUS ELL

radius of curvature = 5.73 inches

radius/diameter = 2.86

total run time = 90.0 hours

initial fitting weight = 26.10 pounds

final fitting weight = 25.46 pounds

total weight loss = 0.64 pounds

weight loss/exposed surface area = 0.0136 psi

$$\text{percent change in weight} = \frac{26.10 - 25.46}{26.10} \times 100 = 2.45\%$$

initial mud properties:

- density = 8.9 pounds/gallon
- absolute viscosity = 6 centipoise
- yield point = 3 pounds/100 square feet

Figure 25 is a plot of the sand grain size distribution after 90 hours of run time.

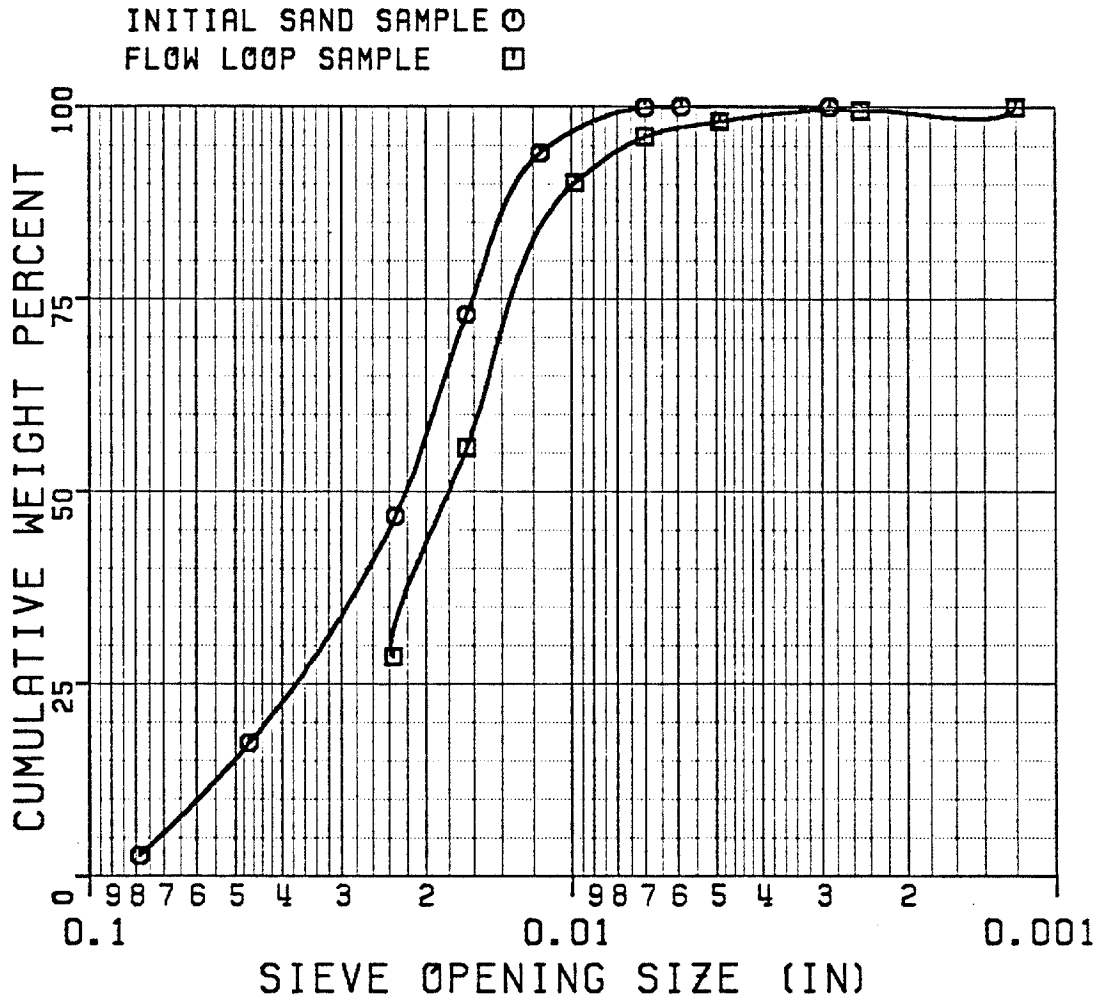

GRAIN SIZE DISTRIBUTION

Figure 25. Grain size distribution of the sand after 90 hours of run time (all samples combined).

TABLE 7

FLOW LOOP DATA FOR THE
SHORT RADIUS ELL

elapsed time (hr)	flowline pressure (psig)	differential pressure (psig)	flowrate (bbl/min)	sand content (%)
0.0	58.5	3.11	8.6	8
17.5	55.0	2.57	8.6	6
41.0	54.9	2.50	9.1	6
65.5	55.3	2.35	-	8
90.0	54.9	2.40	8.9	2
averages	55.7	2.59	8.8	6

average slurry velocity (calculated) = 37.7 feet/second

elapsed time (hr)	upstream temperature (F)	downstream temperature (F)	average temperature (F)
0.0	108.3	107.4	107.8
17.5	172.0	170.7	171.3
41.0	175.7	174.4	175.0
65.5	181.7	180.3	181.0
90.0	160.3	158.6	159.4
averages	159.6	158.3	158.9

TABLE 8

THICKNESS MEASUREMENT LOCATIONS (INCHES)
SHORT RADIUS ELL

OUTSIDE RADIUS (A TO B)

measure point number	1	2	3	4	5
distance from flange face A	1/4	1	1 7/8	2 7/8	3 3/4

measure point number	6	7	8	9	10
distance from flange face A	4 7/8	5 7/8	6 7/8	7 7/8	8 7/8

INSIDE RADIUS (A TO B)

measure point number	1	2	3	4
distance from flange face A	1/2	1 1/2	2 3/4	3 3/4

TABLE 9

ULTRASONIC THICKNESS MEASUREMENT DATA
SHORT RADIUS ELL

BEFORE TESTING/AFTER TESTING (THOUSANDTHS OF AN INCH)

OUTSIDE RADIUS (A TO B)

point number	1	2	3	4	5
top row	620/600	620/600	620/600	620/620	590/580
middle row	630/630	625/620	605/600	590/580	580/555
bottom row	660/645	640/640	620/605	585/570	585/560

point number	6	7	8	9	10
top row	585/580	600/580	605/570	580/545	570/545
middle row	590/560	600/560	605/570	590/545	600/560
bottom row	600/565	620/580	600/570	585/540	580/540

INSIDE RADIUS (A TO B)

point number	1	2	3	4
middle row	585/565	600/570	640/620	600/580

EXPERIMENTAL DATA

PLUGGED TEE

radius of curvature = N/A

radius/diameter = N/A

total run time = 90.0 hours

initial fitting weight = 42.86 pounds

final fitting weight = 41.29 pounds

total weight loss = 1.57 pounds

weight loss/exposed surface area = 0.0222 psi

$$\text{percent change in weight} = \frac{42.86 - 41.29}{42.86} \times 100 = 3.66\%$$

initial mud properties:

density = 9.4 pounds/gallon

absolute viscosity = 2 centipoise

gel strength = 5 pounds/100 square feet

Figure 26 is a plot of the sand grain size distribution after 90 hours of run time.

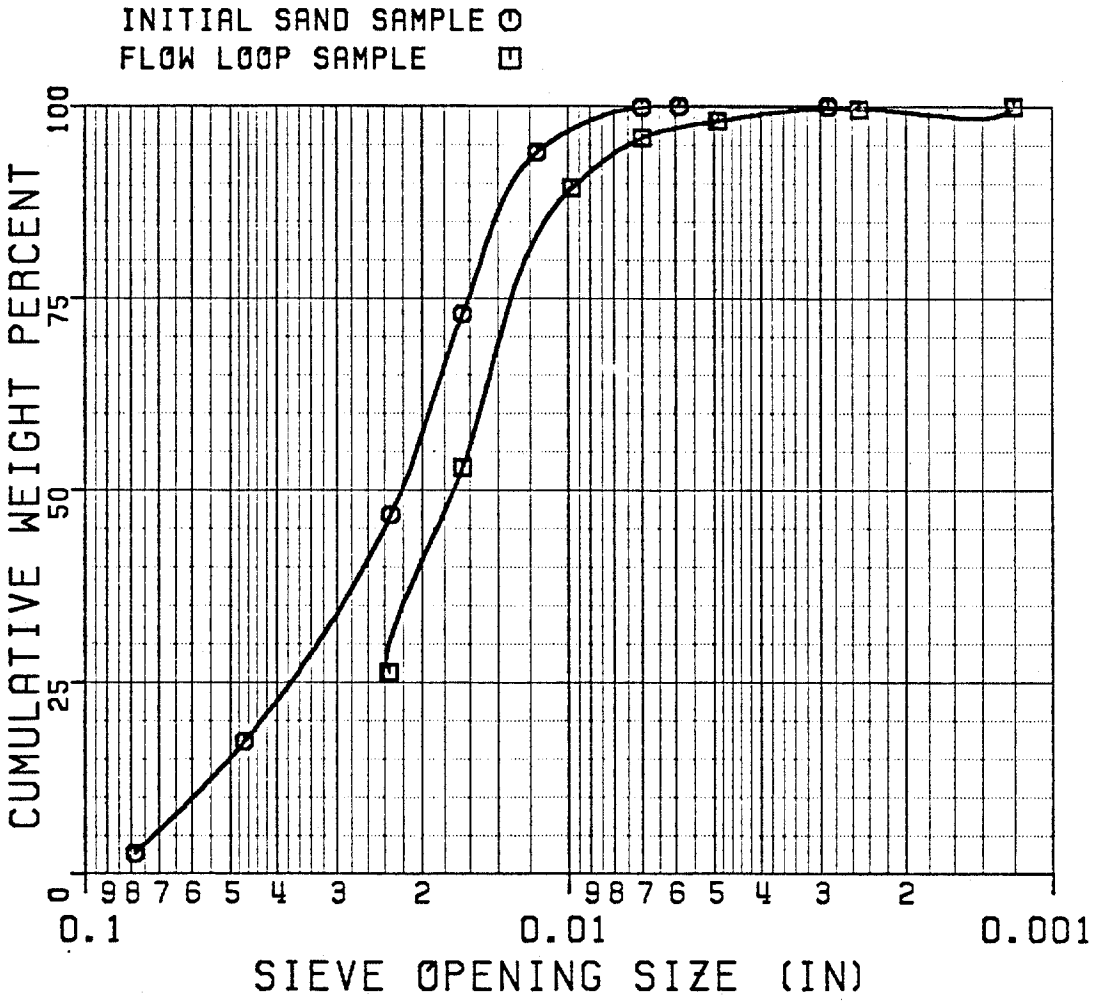

GRAIN SIZE DISTRIBUTION

Figure 26. Grain size distribution of the sand after 90 hours of run time (all samples combined).

TABLE 10

FLOW LOOP DATA FOR THE PLUGGED TEE

elapsed time (hr)	flowline pressure (psig)	differential pressure (psig)	flowrate (bbl/min)	sand content (%)
0.0	55.2	6.80	8.9	18
22.5	51.1	6.33	9.8	16
47.0	52.0	7.26	-	1
66.0	51.7	7.39	10.3	3
73.5	52.7	7.34	10.0	3
90.0	50.2	7.34	-	5
averages	51.5	6.78	9.8	8

average slurry velocity (calculated) = 41.9 feet/second

elapsed time (hr)	upstream temperature (F)	downstream temperature (F)	average temperature (F)
0.0	133.8	132.4	133.1
22.5	155.6	153.8	154.7
47.0	95.0	93.5	94.3
66.0	152.8	151.4	152.1
73.5	154.9	153.2	154.0
90.0	201.8	199.7	200.8
averages	149.0	147.3	148.2

TABLE 11

THICKNESS MEASUREMENT LOCATIONS (INCHES)
PLUGGED TEE

OUTSIDE RADIUS (A TO B)

measure point number	1	2	3	4	5
distance from flange face A	1/4	1	2	3	4

measure point number	6	7	8	9
distance from flange face A	5	6	7	8

INSIDE RADIUS (A TO C)

measure point number	1	2	3	4
distance from flange face A	3/8	1 1/2	3 1/4	4

INSIDE RADIUS (B TO C)

measure point number	1	2	3	4
distance from flange face B	3/4	2	3 1/4	4 1/4

TABLE 12

ULTRASONIC THICKNESS MEASUREMENT DATA
PLUGGED TEE

BEFORE TESTING/AFTER TESTING (THOUSANDTHS OF AN INCH)

OUTSIDE (A TO B)

point number	1	2	3	4	5
top row	665/620	640/625	640/620	645/640	680/625
middle row	640/600	600/600	590/580	600/580	600/585
bottom row	580/560	580/565	580/580	585/565	600/580

point number	6	7	8	9
top row	685/650	645/630	640/620	640/620
middle row	605/605	685/680	585/570	620/600
bottom row	585/570	580/560	580/560	580/560

INSIDE RADIUS (A TO C)

point number	1	2	3	4
top row	600/570	640/580	620/520	600/440
middle row	620/585	620/620	620/420	605/435
bottom row	585/580	600/600	695/385	660/420

INSIDE RADIUS (B TO C)

point number	1	2	3	4
top row	620/570	640/660	700/480	620/495
middle row	650/600	610/600	680/460	640/490
bottom row	600/600	610/600	640/400	600/495

EXPERIMENTAL DATA

LONG RADIUS ELL

radius of curvature = 7.00 inches

radius/ diameter = 3.50

total run time = 90.0 hours

initial fitting weight = 22.59 pounds

final fitting weight = 21.13 pounds

total weight loss = 1.46 pounds

weight loss/exposed surface area = 0.0258 psi

$$\text{percent change in weight} = \frac{22.59 - 21.13}{22.59} \times 100 = 6.46\%$$

initial mud properties:

density = 9.0 pounds/gallon

absolute viscosity = 5 centipoise

yield point = 4 pounds/100 square feet

Figure 27 is a plot of the sand grain size distribution after 90 hours of run time.

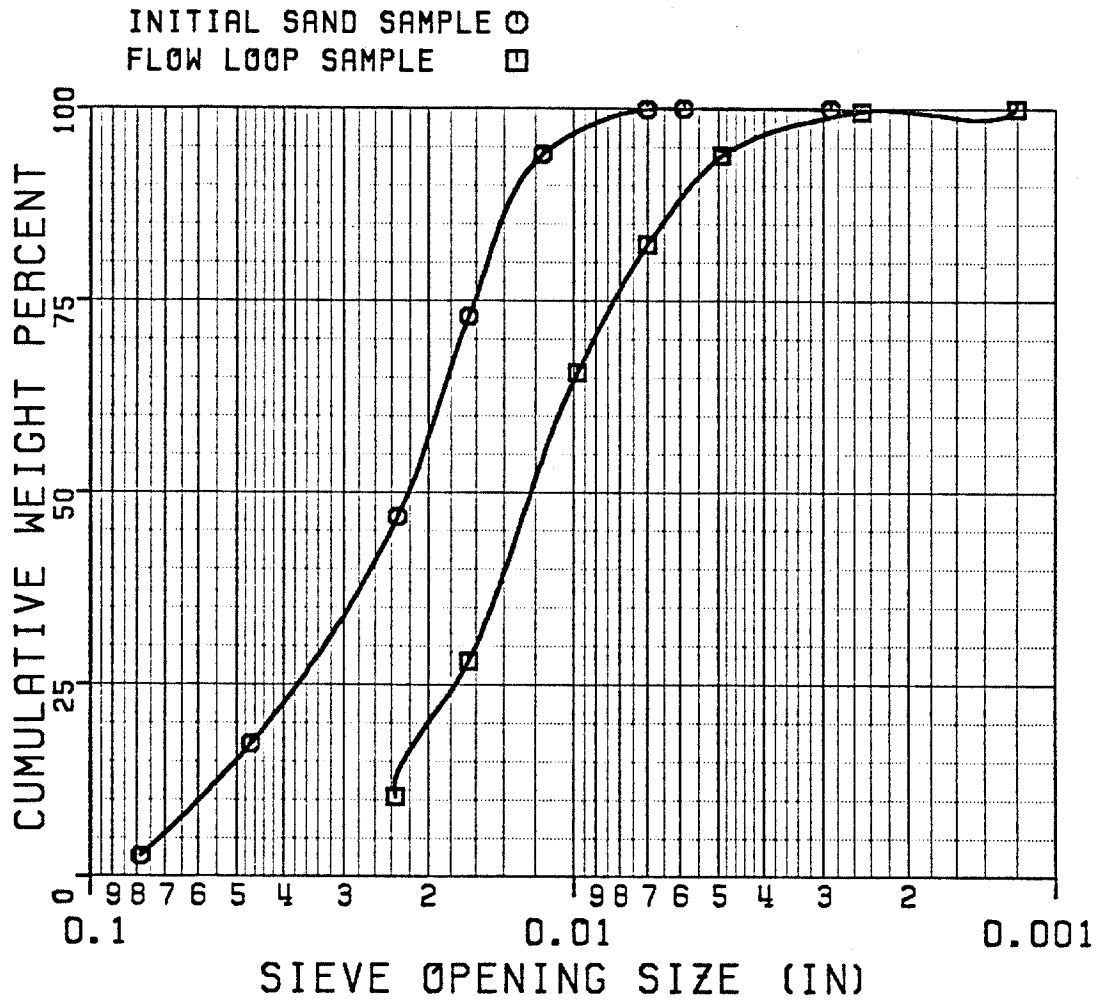

GRAIN SIZE DISTRIBUTION

Figure 27. Grain size distribution of the sand after 90 hours of run time (all samples combined).

TABLE 13

FLOW LOOP DATA FOR THE
LONG RADIUS ELL

elapsed time (hr)	flowline pressure (psig)	differential pressure (psig)	flowrate (bbl/min)	sand content (%)
0.0	46.0	1.27	11.2	3
6.0	43.9	1.18	-	5
30.0	40.3	1.13	11.4	5
39.5	42.2	1.13	-	-
64.0	42.8	1.14	11.1	2
90.0	43.5	1.18	10.9	1
averages	43.1	1.17	11.2	3

average slurry velocity (calculated) = 47.8 feet/second

elapsed time (hr)	upstream temperature (F)	downstream temperature (F)	average temperature (F)
0.0	107.9	106.4	107.2
6.0	171.3	170.3	170.8
30.0	180.7	179.6	180.2
39.5	122.7	121.1	121.9
64.0	116.5	114.1	115.3
90.0	207.1	206.2	206.6
averages	151.0	149.6	150.3

TABLE 14

THICKNESS MEASUREMENT LOCATIONS (INCHES)
LONG RADIUS ELL

OUTSIDE RADIUS (A TO B)

measure point number	1	2	3	4
distance from flange face A	1/4	7/8	1 7/8	2 7/8

measure point number	5	6	7	8
distance from flange face A	3 7/8	4 7/8	5 3/8	6 7/8

measure point number	9	10	11	12
distance from flange face A	7 7/8	8 7/8	9 7/8	10 1/2

INSIDE RADIUS (A TO B)

measure point number	1	2	3
distance from flange face A	3/4	1 3/4	2 3/4

measure point number	4	5	6
distance from flange face A	3 3/4	4 3/4	5 5/8

TABLE 15

ULTRASONIC THICKNESS MEASUREMENT DATA
LONG RADIUS ELL

BEFORE TESTING/AFTER TESTING (THOUSANDTHS OF AN INCH)

OUTSIDE RADIUS (A TO B)

point number	1	2	3	4
top row	460/420	450/405	440/380	435/340
middle row	480/440	460/400	460/360	445/320
bottom row	480/460	480/420	480/385	480/325

point number	5	6	7	8
top row	430/305	445/300	440/270	460/260
middle row	445/300	440/250	420/220	440/205
bottom row	455/325	440/260	440/245	425/220

point number	9	10	11	12
top row	480/245	485/305	500/240	490/240
middle row	440/160	440/210	440/160	480/140
bottom row	420/180	420/180	435/150	430/120

TABLE 15-CONTINUED

INSIDE RADIUS (A TO B)

point number	1	2	3
top row	545/540	585/560	565/550
middle row	540/505	530/500	545/525
bottom row	490/480	520/520	540/500

point number	4	5	6
top row	565/540	540/505	500/480
middle row	565/540	540/505	500/480
bottom row	560/500	560/535	520/500

EXPERIMENTAL DATA

VORTICE-ELL

radius of curvature = 4.66 inches

radius/diameter = 2.33

total run time = 90.0 hours

initial fitting weight = 61.85 pounds

final fitting weight = 59.96 pounds

total weight loss = 1.89 pounds

weight loss/exposed surface area = 0.0222 psi

$$\text{percent change in weight} = \frac{61.85 - 59.96}{61.85} \times 100 = 3.06\%$$

initial mud properties:

- density = 10.0 pounds/gallon
- absolute viscosity = 6 centipoise
- yield point = 3 pounds/100 square feet

Figure 28 is a plot of the sand grain size distribution after 90 hours of run time.

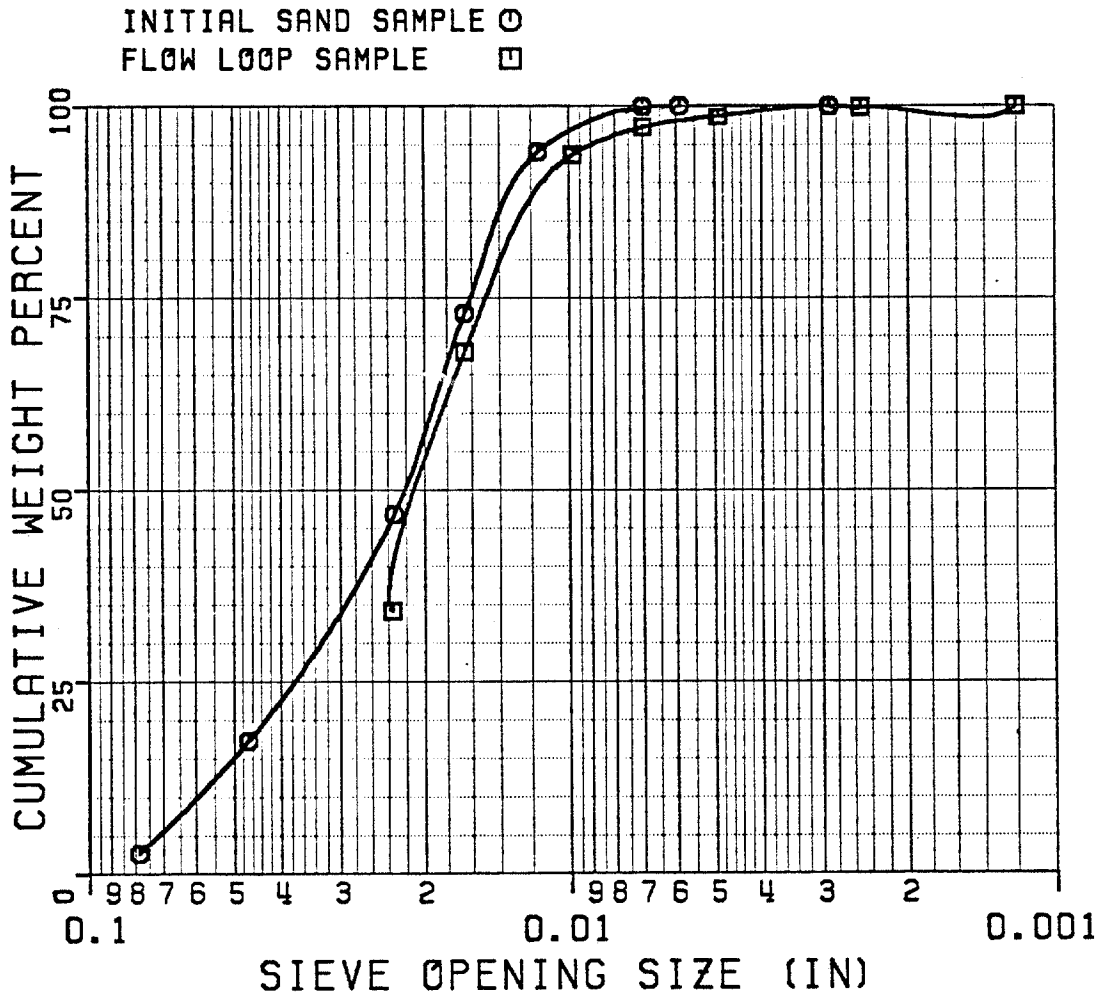

GRAIN SIZE DISTRIBUTION

Figure 28. Grain size distribution of the sand after 90 hours of run time (all samples combined).

TABLE 16

FLOW LOOP DATA FOR THE VORTICE-ELL

elapsed time (hr)	flowline pressure (psig)	differential pressure (psig)	flowrate (bbl/min)	sand content (%)
0.0	51.8	8.34	11.1	20
19.0	48.6	7.32	10.4	5
44.0	50.0	7.56	10.5	13
67.0	47.0	8.54	10.8	6
90.0	51.2	7.90	10.8	-
averages	49.7	7.93	10.7	11

average slurry velocity (calculated) = 45.9 feet/second

elapsed time (hr)	upstream temperature (F)	downstream temperature (F)	average temperature (F)
0.0	134.9	133.3	134.1
19.0	206.2	205.4	205.8
44.0	178.8	177.8	178.3
67.0	190.6	189.5	190.1
90.0	193.6	192.7	193.2
90.0	193.6	192.7	193.2
averages	180.8	179.7	180.3

TABLE 17

THICKNESS MEASUREMENT LOCATIONS (INCHES)
VORTICE-ELL

OUTSIDE RADIUS (A TO B)

measure point number	1	2	3	4	5
distance from flange face A	3/4	1 3/4	4 7/8	5 7/8	6 7/8

measure point number	6	7	8	9	10
distance from flange face A	7 7/8	9	10	11	12 1/8

measure point number	11	12	13	14	15
distance from flange face A	13 1/8	14 1/8	15 1/8	16 1/8	16 7/8

INSIDE RADIUS (A TO B)

measure point number	1	2	3
distance from flange face A	1/2	1 1/2	2 1/2

measure point number	4	5	6
distance from flange face A	3 1/2	4 1/2	5

TABLE 18

ULTRASONIC THICKNESS MEASUREMENT DATA
VORTICE-ELL

BEFORE TESTING/AFTER TESTING (THOUSANDTHS OF AN INCH)

OUTSIDE RADIUS (A TO B)

point number	1	2	3	4	5
top row	645/620	640/620	660/660	640/600	620/540
middle row	660/540	580/540	700/680	630/590	620/500
bottom row	665/560	585/560	640/610	585/540	580/520

point number	6	7	8	9	10
top row	650/600	645/600	680/600	645/545	640/560
middle row	605/540	605/545	690/580	700/560	620/540
bottom row	605/550	600/540	600/585	620/550	620/540

point number	11	12	13	14	15
top row	620/545	620/540	720/440	605/235	625/425
middle row	620/540	620/560	620/380	605/300	600/360
bottom row	600/540	660/600	585/345	575/300	560/360

TABLE 18-CONTINUED

INSIDE RADIUS (A TO B)

point number	1	2	3
top row	580/565	580/540	545/440
middle row	600/580	560/560	580/480
bottom row	580/560	580/560	580/480

point number	4	5	6
top row	545/400	540/425	575/460
middle row	580/440	560/445	575/460
bottom row	565/460	565/465	560/450

The results of the welded fitting test runs are presented on the following pages.

WELDED SHORT RADIUS ELL

Erosion Patterns

OUTSIDE RADIUS

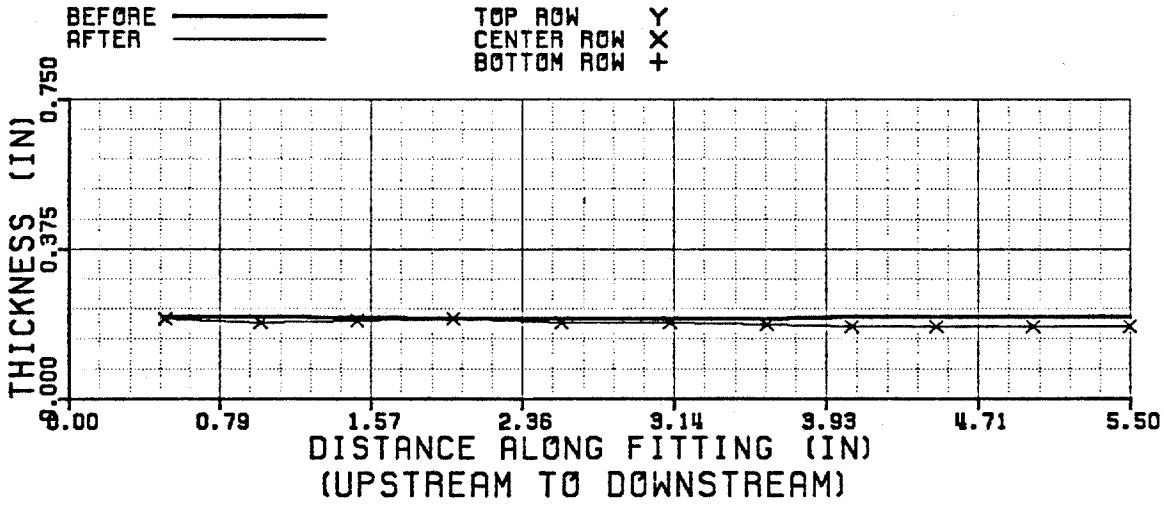

WELDED SHORT RADIUS ELL
OUTSIDE (A TO B)

WELDED SHORT RADIUS ELL

(SECOND RUN)

Erosion Patterns

OUTSIDE RADIUS

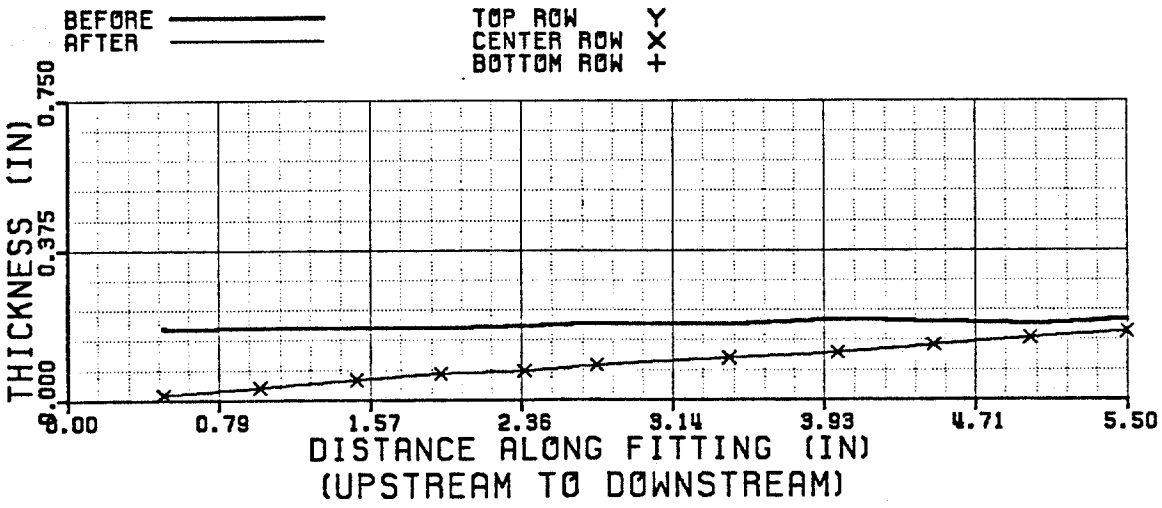

WELDED SHORT RADIUS ELL
OUTSIDE (A TO B)
(SECOND RUN)

WELDED PLUGGED TEE

Erosion Patterns

INSIDE RADIUS

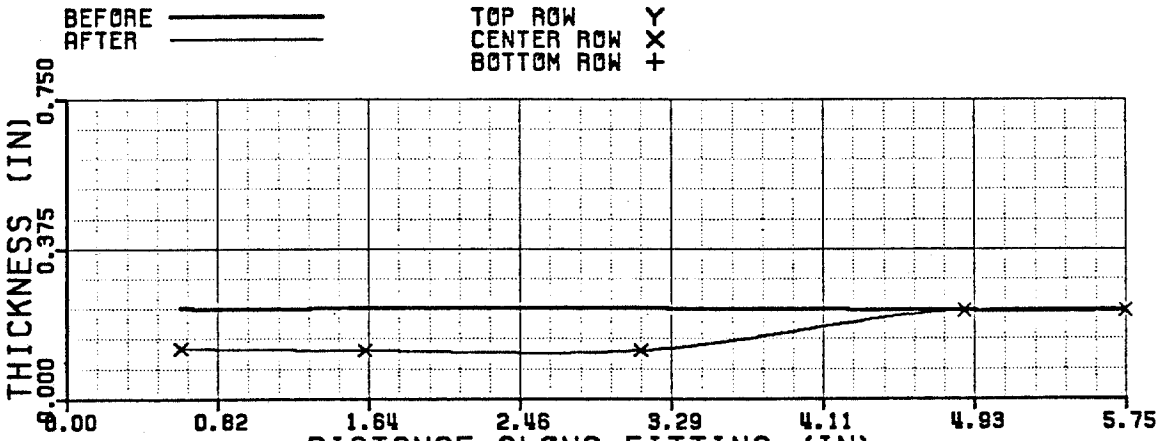

WELDED PLUGGED TEE
INSIDE (A TO C)

INSIDE RADIUS

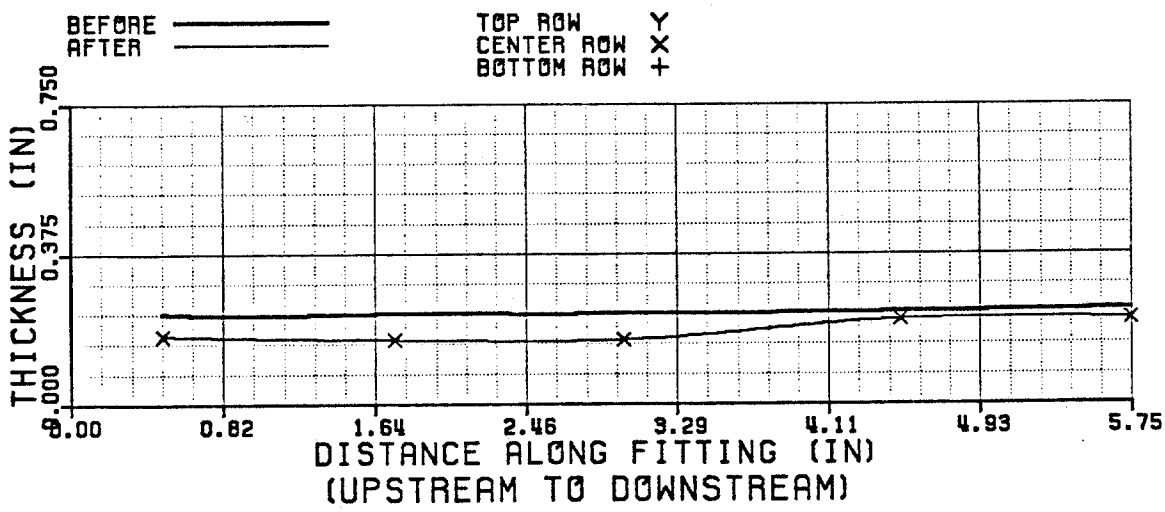

WELDED PLUGGED TEE
INSIDE (B TO C)

OUTSIDE RADIUS

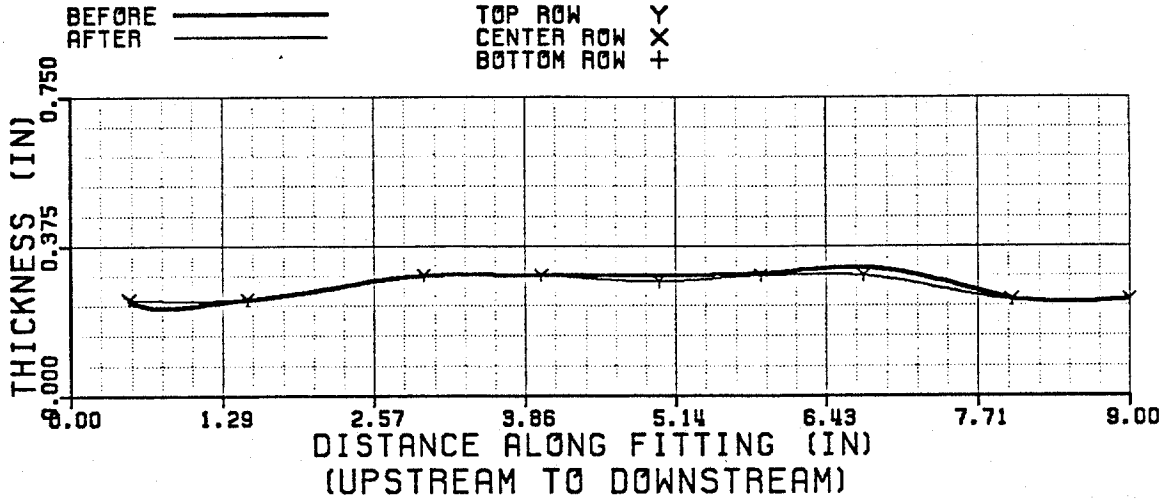

WELDED PLUGGED TEE
OUTSIDE (A TO B)

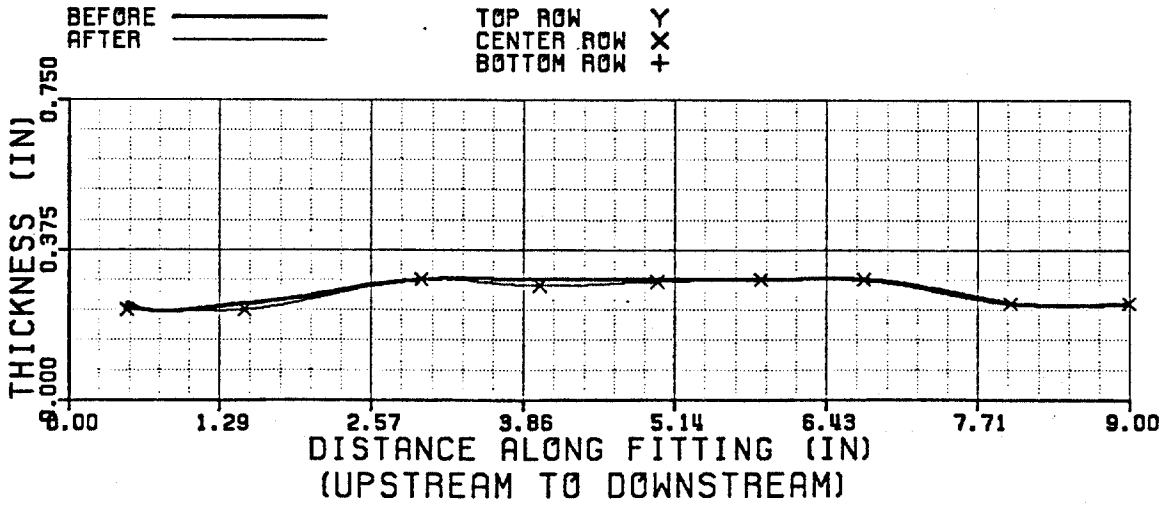

WELDED PLUGGED TEE
OUTSIDE (A TO B)

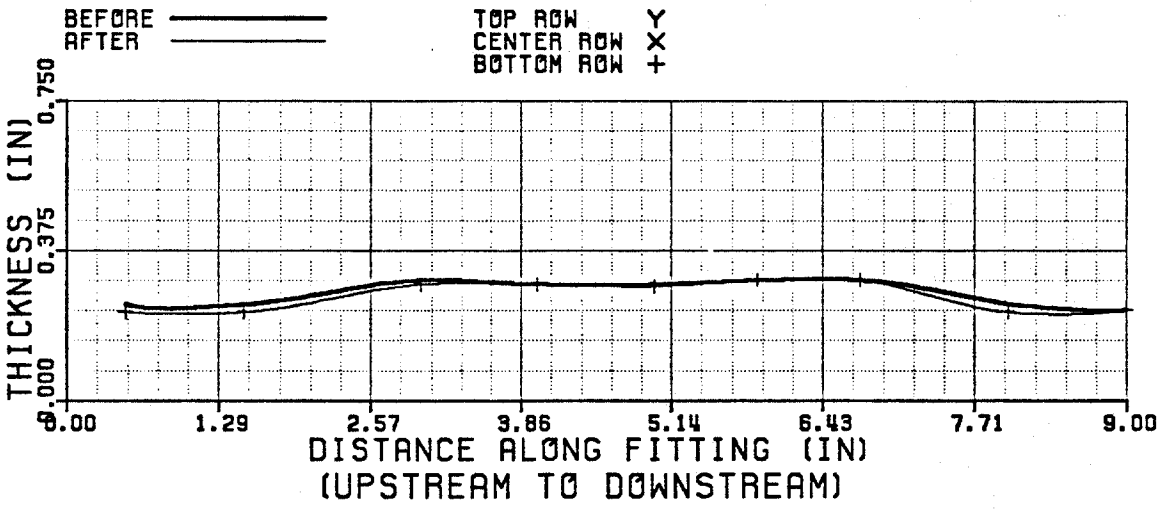

WELDED PLUGGED TEE
OUTSIDE (A TO B)

VITA

Stephen Arthur Rohleder, the third child of John and Roberta Rohleder, was born on October 15, 1958. He was raised in the Chicago suburb of Northbrook, Illinois and attended Loyola Academy High School in Wilmette, Illinois. In 1976 he enrolled at the University of Wisconsin in Madison and, in 1981, graduated with a Bachelor of Science degree in Agricultural Engineering. In July of that year, he began working for Schlumberger Well Services in New Iberia, Louisiana. Six months later he was promoted from Junior Field Engineer to Field Engineer. Due to a slowdown in business, he was laid off in May, 1982. In the Spring semester of 1983, he enrolled in graduate school at Tulane University in New Orleans, Louisiana. After 1 semester, he transfered to Louisiana State University where he received a Master of Science degree in petroleum engineering. Stephen is presently a Junior member of the Society of Petroleum Engineers.